Quaternary Science Reviews 268 (2021) 107115

Contents lists available at ScienceDirect

Quaternary Science Reviews

journal homepage: www.elsevier.com/locate/quascirev

A multi-decadal geochemical record from Rano Aroi (Easter Island/Rapa Nui): Implications for the environment, climate and humans during the last two millennia

Marco Roman [a, *], David B. McWethy [b], Natalie M. Kehrwald [c], Evans Osayuki Erhenhi [a], Amy E. Myrbo [d], José M. Ramirez-Aliaga [e], Anibal Pauchard [f, g], Clara Turetta [h], Carlo Barbante [a, h], Matthew Prebble [i, j], Elena Argiriadis [a, h], Dario Battistel [a, h]

[a] Department of Environmental Sciences, Informatics and Statistics, Ca' Foscari University of Venice, Via Torino 155, 30170, Venezia Mestre, Italy
[b] Department of Earth Sciences, Montana State University, Bozeman, MT, United States
[c] Geosciences and Environmental Change Science Center, U.S. Geological Survey, Denver, CO, United States
[d] St. Croix Watershed Research Station, Science Museum of Minnesota, 16910 152nd St North, Marine on St. Croix, MN, 55047, United States
[e] Grupo Interdisciplinario de Investigación Avanzada, Universidad de Playa Ancha, Valparaíso, Chile
[f] Laboratorio de Invasiones Biológicas (LIB), Facultad de Ciencias Forestales, Universidad de Concepción, Concepción, Chile
[g] Institute of Ecology and Biodiversity, Santiago, Chile
[h] Institute of Polar Sciences – National Research Council (ISP-CNR), Via Torino 155, 30170, Venezia Mestre, Italy
[i] School of Earth and Environment, College of Science, University of Canterbury, Christchurch, 8041, New Zealand
[j] Department of Archaeology and Natural History, School of Culture, History and Language, College of Asia and the Pacific, Australian National University, Canberra, ACT, 2601, Australia

ARTICLE INFO

Article history:
Received 23 December 2020
Received in revised form
24 July 2021
Accepted 25 July 2021
Available online 14 August 2021

Handling Editor: I. Hendy

Keywords:
Anthropocene
Paleoclimatology
Southern Pacific
Rapa Nui
Wetland
Inorganic geochemistry

ABSTRACT

The small and remote Easter Island (Rapa Nui) has a complex and still partially unknown history of human colonization and interactions with the environment. Previous research from sedimentary archives collected in the three freshwater bodies of Rapa Nui document dramatic environmental changes over the last two millennia. Yet, the characteristics of sediments and paleoenvironmental records are challenging to interpret, mainly due to poor temporal resolution, hiatuses and sediment mixing.

In this study, we reconstruct past changes in lithogenic inputs, weathering processes, redox conditions, productivity and water levels in the Rano Aroi wetland over the last 2000 years through the determination of major, trace and rare earth elements in a new peat core collected in 2017. The chronology is based on 8 ^{14}C AMS dates for the upper 1.5 m and provides decadal to multi-decadal resolution which is unprecedented for the island of Rapa Nui. The multielemental proxies depict seven distinct chronological phases marked by well-defined geochemical transitions. With only a few minor fluctuations, climate conditions were dry and the mire was mildly anoxic during the first millennium (0–1000 CE) to the arrival of the first Polynesians in Rapa Nui (800–1300 CE) and until ~1400 CE, followed by wetter conditions afterwards. The record documents with unprecedented accuracy and resolution intense droughts occurring during the middle Little Ice Age between 1520 and 1710 CE, which may have been exacerbated by human activities and triggered dramatic cultural shifts. During the interval of first contact between the Rapanuis and Europeans, the climate changed to wetter conditions, followed by intense precipitations between 1790 and 1900 CE.

1. Introduction

Easter Island (Rapa Nui) is a small, remote island located in the southeastern Pacific Ocean that was colonized by Polynesians between 800 and 1300 CE (Rull, 2016 and references therein). Rapa Nui is a site of substantial archaeological interest due to the hundreds of massive megalithic statues, known as moai, built by the inhabitants of the island until approximately the end of the 18th century (Sherwood et al., 2019). These statues are associated with

* Corresponding author.
E-mail address: marco.roman@unive.it (M. Roman).

https://doi.org/10.1016/j.quascirev.2021.107115
0277-3791/

oral traditions of the "Ahu-Moai". Between the mid-16th and late-18th centuries, the "Ahu-Moai" was replaced by the Birdman Cult leading to a profound change in the social organization and religious practices of the Rapanuis population (Edwards and Edwards, 2013). The timing and the causes of the profound cultural transformation at Rapa Nui and possible links to environmental and ecological changes is still actively debated (Diamond, 2005; Flenley and Bahn, 2003; Hunt, 2007; Hunt and Lipo, 2006, 2011; Mieth and Bork, 2010; Rull et al., 2018). Resolving these linkages remains elusive, partially due to the difficulty of obtaining high-resolution records with a robust chronology from the limited paleoenvironmental and paleoecological archives available from Rapa Nui.

Here we analyze the geochemical composition of the peat and sediments from the Rano Aroi wetland over the last 2000 years to better understand the sequence of biogeochemical changes prior to and after both Polynesian and European arrival. Previous paleoenvironmental studies focused on sedimentary archives collected from the three freshwater bodies within the island's calderas: Rano Raraku, Rano Kau and Rano Aroi (Azizi and Flenley, 2008; Cañellas-Boltà et al., 2016, 2013; Dumont et al., 1998; Horrocks et al., 2012; Mann et al., 2008; Rull et al., 2010; Sáez et al., 2009 among others). These three sites have different characteristics due to their underlying bedrock composition and settings (Table 1). Previous research from these sites documented dramatic environmental changes such as droughts, yet interpreting the sequence and timing of environmental change from paleoenvironmental records has been difficult for a number of reasons (e.g. poor temporal resolution, hiatuses, sediment mixing) (Rull, 2021).

Rano Raraku is adjacent to the main quarry where the moais were carved, and is one of the most studied locations on the island for what concerns paleoenvironmental reconstructions (Cañellas-Boltà et al, 2013, 2016, 2013; Horrocks et al., 2012; Rull, 2016; Sáez et al., 2009). However, Rano Raraku sediments from the last two millennia may incorporate a hiatus and/or surface sediment mixing due to high levels of bioturbation, desiccation and weathering. Any connections between this lake desiccation and water use for the quarry are currently unknown. Other paleoecological research focused on the lacustrine deposits of the large crater in the southwest corner of Rapa Nui named Rano Kau (Butler and Flenley, 2010; Gossen, 2007; Horrocks et al, 2012, 2013). However, sedimentation is also problematic at Ranu Kau in part due to floating vegetation mats comprised primarily of living *Scirpus californicus*, that cover much of the lake surface. When fragments of these mats die or degrade, they appear to sink to the basin mud-water interface, mixing with older and younger sediments. This mixing influences the dating of these archives and can result in depth-age reversals and chronological inconsistencies (Butler et al., 2004). For this reason, as well as the overturning of the mats through time, depth-age chronologies for Rano Kau are complicated and lack adequate resolution, especially for the upper sediments.

Sediments from the Rano Aroi wetland (430 m asl), adjacent to the highest point of Rapa Nui, the Maunga Terevaka summit (511 m asl), received initial interest from researchers (Flenley et al., 1991; Flenley and King, 1984). With the exception of a single study (Peteet et al., 2003), the wetland then received less attention than Rano Kau and Rano Raraku over the next 20 years due to the potential human disturbance that may have had compromised sedimentation. Rano Aroi has been only recently been reconsidered as a promising paleoecological archive (Horrocks et al., 2015; Margalef et al, 2013, 2014, 2013; Rull et al., 2015). These recent studies demonstrated that the Rano Aroi wetland represents the accumulation of a continuous sediment sequence spanning the last two millennia in less than 1.5 m of sediments. The previous depth-age chronologies for Rano Aroi exhibit several age reversals and considerable chronological uncertainty. The Rano Aroi core used in this study provides a robust and continuous paleoenvironmental record for the last 2000 years with the highest temporal resolution (decadal) of any previous dataset from Rapa Nui to date.

The Rano Aroi wetland was previously investigated for paleobotanical proxies (Flenley et al., 1991; Horrocks et al., 2015; Peteet et al., 2003; Rull et al., 2015), stable isotopes (Margalef et al., 2013) and elemental concentrations (Margalef et al, 2013, 2014). Margalef et al. (2014) demonstrated the potential use of elemental tracers in conjunction with pollen and stable isotopes in the Rano Aroi peat cores to reconstruct vegetation changes, mineral input and biogeochemical processes. However, the authors focused on such changes over the last ~70000 years and provided limited data on the environmental and climatic evolution recorded in Rano Aroi over the interval spanning the Polynesian settlement of Rapa Nui. Rull et al. (2015) investigated peat core sections spanning the past three millennia, analyzing pollen and charcoal sequences in conjunction with bulk peat total carbon (TC) and total nitrogen (TN), yet the geochemistry of the last millennium was limited to TC, TN and $\delta^{13}C$ and $\delta^{15}N$ isotopic composition with multi-decadal to centennial resolution. Horrocks et al. (2015) studied pollen and microfossils in a peat core from Rano Aroi spanning the last ~30000 years, providing evidence for vegetational changes induced by human activities including forest clearance between 1240 and 1610 CE, and horticulture after 1670 CE.

Overall, trace elements (TE) have been underutilized in previous paleoclimate studies at Rapa Nui, particularly for the last two millennia, but do have a high potential for disentangling the

Table 1
Key characteristics of the three main water bodies and corresponding archives from the past 2000 y in Rapa Nui.

	Rano Aroi	Rano Raraku	Rano Kau
Coordinates	−27.09, −109.37	−27.12, −109.29	−27.18, 109.43
Elevation (m)	425	75	110
Size (km^2)	0.022	0.11 (catchment 0.35)	1.2
Hydrology	Mire fed more by rainfall than groundwater	Shallow lake (max depth tens cm to 4 m)	Lake, 10 m of water between floating vegetation mats and sediment
Sediments	Reddish peat/detritus, coarse plant remains, narrow clay layers	Silicate-rich silty peat	Unconsolidated coarse organic detritus, clay layer
Chronology	Compressed in 1.5 m, consistent	Compressed in <25 cm, two hiatuses, complicated by contamination with older carbon and age reversals provided by *Scirpus* sp. roots	Inconsistent between different cores, complicated by floating vegetation mat
Notes	Creation of a small dam at the SE edge in the 1920s, complete desiccation in 2018	Insertion of a pipe in 1958 could have drained out much of the water at the time	
References	Flenley et al. (1991); Flenley and King (1984); Horrocks et al. (2015); Margalef et al. (2014), 2013; Rull et al. (2015)	Cañellas-Boltà et al. (2016), 2012; Dumont et al. (1998); Flenley and Bahn (2003); Geller (1992); Horrocks et al. (2012); Sáez et al. (2009)	Bowdery (2015); Butler et al. (2004); Butler and Flenley (2010); Gossen (2007); Horrocks et al. (2013)

complex interactions between regional climate, local environmental changes and anthropogenic pressure and associated reactions (Allan et al., 2013; Ferrat et al., 2012; Margalef et al., 2014). The absolute concentrations and ratios of specific TE can preserve a geochemical signature of processes or conditions such as precipitation regimes, minerogenic and biogenic input sources and intensities, changes in the water table, droughts, redox state and nutrients mobility. Periods characterized by an enhanced exogenous input typically entail an increase in the concentration of lithogenic elements associated with fine dust from atmospheric depositions and/or coarser particles transported through hydraulic erosion. Some elements, such as Al and Ti, are chemically inert and have very low mobility in the peat, and can thus can be adopted as proxies of lithogenic inputs and normalizing elements (Biester et al., 2012; Le Roux et al., 2006; Muller et al., 2008). Others like K and Na are prone to chemical weathering. Variations in the K/Al ratio can indicate the relative prevalence of physical versus chemical weathering in sediments (Arnaud et al., 2016), but also the uptake and recycling of nutrients by plants in the mire (Biester et al., 2012). The interaction between the water table and vegetation can impact the processes of primary production, humification and mineralization, which in turn are strongly associated with the redox state of the mire (and pH in minerothrophic systems) (Beer et al., 2008; Chesworth et al., 2006). Furthermore, different redox-sensitive elements such as Fe, Mn and Ce may track changes in solubility rates and equilibrium (Chesworth et al., 2006; Damman, A.W.H.; Tolonen, K.; Sallantaus, 1992; Davranche et al., 2017; Margalef et al., 2013; Shotyk, 1988). Calcium is another element sensitive to a combination of ion inputs from groundwater, changes in the redox-pH state and intensive uptake and recycling within the organic substrate (Biester et al., 2012; Shotyk et al., 2002). Other elements such as P are strongly associated with nutrient intake (often proposed as a limiting factor for plant growth) and are affected by redox-dependent adsorption onto Mn/Fe (oxyhydr)oxides, with complex dynamics that are not yet fully understood (Kellogg and Bridgham, 2003; Tipping et al., 2014). Rare earth elements (REE) exhibit very similar geochemical dynamics among themselves, but with slight differences in the relative solubility which can be tracked through selected ratios between light and heavy elements (LREE and HREE, respectively) (Nelson et al., 2003).

Trace elements-derived proxies are typically affected by or indicative of multiple geochemical processes. The best strategy for defining the most appropriate proxy for a geochemical process is to analyze multiple elements with a quantitative approach, and then integrate these results with more orthodox paleoenvironmental proxies such as sediment stratigraphy, palynology, stable isotopes etc.).

In this study we reconstruct the paleoenvironmental changes in Rapa Nui using the geochemical composition and associated changes in a new high resolution (decadal) peat sequence from Rano Aroi that encompasses the past two millennia. Trace elements and REE present an extended set of geochemical proxies including elemental ratios (K/Al, Fe/Al, Ca/Ti, Mn/Fe, P/Al), cerium anomaly (δCe) and REE fractionation indexes ($(La/Yb)_N$, $(Gd/Yb)_N$, $(La/Sm)_N$). The dataset complements the organic carbon content (OC%) and the sediment accumulation rates to calculate representative variables by principal component analysis (PCA). With the support of the PCA synthesis and cluster analysis (CA) results, we detected seven geochemically distinct phases. We interpret and discuss these phases within the framework of previous paleoecological findings and archaeological evidence to address the following key questions: (a) what are the most significant drivers of biogeochemical and hydrological changes at Rano Aroi? (b) how did the paleohydrology and erosional processes at Rano Aroi change in response to human arrival on Rapa Nui? (c) Did cultural shifts following human arrival lead to significant changes in the environment or *vice versa*?

1.1. Regional setting

Rapa Nui is a small island (~163 km^2) located in southeast Polynesia (27°09′S, 109°26′W) (Fig. 1). The climate is oceanic and subtropical, with a mean annual temperature of ~21 °C and average monthly temperatures ranging between 18 °C in August and 24 °C in January (Mann et al., 2008). The annual rainfall in the island ranges from ~1100 mm in the coastal areas to >1500 mm in the upper elevations, with a minimum average of 70–80 mm per month in November–December and a maximum of 100–130 mm per month in April–June (Herrera and Custodio, 2008). The increase in precipitation during the Austral fall-winter is driven by a weakening and northward migration of the South Pacific Anticyclone. This weakening leads to the predominance of westerlies loaded with moisture from their passage through the South Pacific Convergence Zone, otherwise prevented during the austral spring/summer (Sáez et al., 2009). Modern precipitation may exhibit a considerable interannual variability, ranging from 500 mm per year to >1800 mm per year, which appears to be unrelated to the cyclicity of the El Niño Southern Oscillation (ENSO) (Azizi and Flenley, 2008). The general influence of ENSO on the climate of Rapa Nui is still controversial. Some analyses reported that the interannual variability of atmospheric temperature, sea surface temperature and rainfall is near zero on the island (MacIntyre, 2001), whereas other studies report spectral correspondence between ENSO and local sea surface temperature variations (Glynn et al., 2003; Mucciarone and Dunbar, 2003) or wind regimes (Anderson et al., 2006). Examination of data from the past 70 years suggests that there is no clearrelationship between rainfall in Rapa Nui and the Southern Oscillation Index (SOI) (Fig. S1), except for the indication that either way strong ENSO phases do not promote precipitations in the island. Rapa Nui is consistently windy during the entire year. The impact of subtropical cyclones is very rare, with the last cyclone occurring in 2015 (Cyclone Katie).

Three freshwater bodies exist on Rapa Nui: the lakes of Rano Raraku and Rano Kau and the Aroi mire (Table 1). Each wetland is contained in the caldera of one of the three volcanoes that formed the island, whose bedrock is mainly composed of basaltic lava flows, porfiric olivinic tholeiite and hawaiite, covered by andosols (Baker et al., 1974; Ferrán et al., 2004; Margalef et al., 2014).

The crater containing Rano Aroi is close to the Maunga Terevaka, the highest summit of the island (511 m asl). The Rano Aroi wetland is ~150 m in diameter (0.13 km^2) at 430 m elevation. The surface vegetation of Rano Aroi primarily consists of *Scirpus californicus* and *Polygonum acuminatum* (Rull et al., 2015). The surrounding landscape consists of grassland and non-native eucalyptus forest introduced ~50 years ago (Cañellas-Boltà et al., 2013; Zizka, 1991). The Rano Aroi wetland system is fed by a perched spring connected to the main island aquifer (Herrera and Custodio, 2008; Margalef et al, 2013, 2014) as well as input from rainfall. The water level is controlled by groundwater input influenced by seasonal variations in precipitation and, in recent decades, water control related to an artificial outlet (see Fig. 1) constructed in the 1960s (Herrera and Custodio, 2008; Rull et al., 2015). The geomorphology, soil and landforms of the island are strongly controlled by past volcanic activity and are composed of a volcanic substrate of basalts, trachytes and peralkaline rhyolites (Gioncada et al., 2010; Gonzalez-Ferran, 1987).

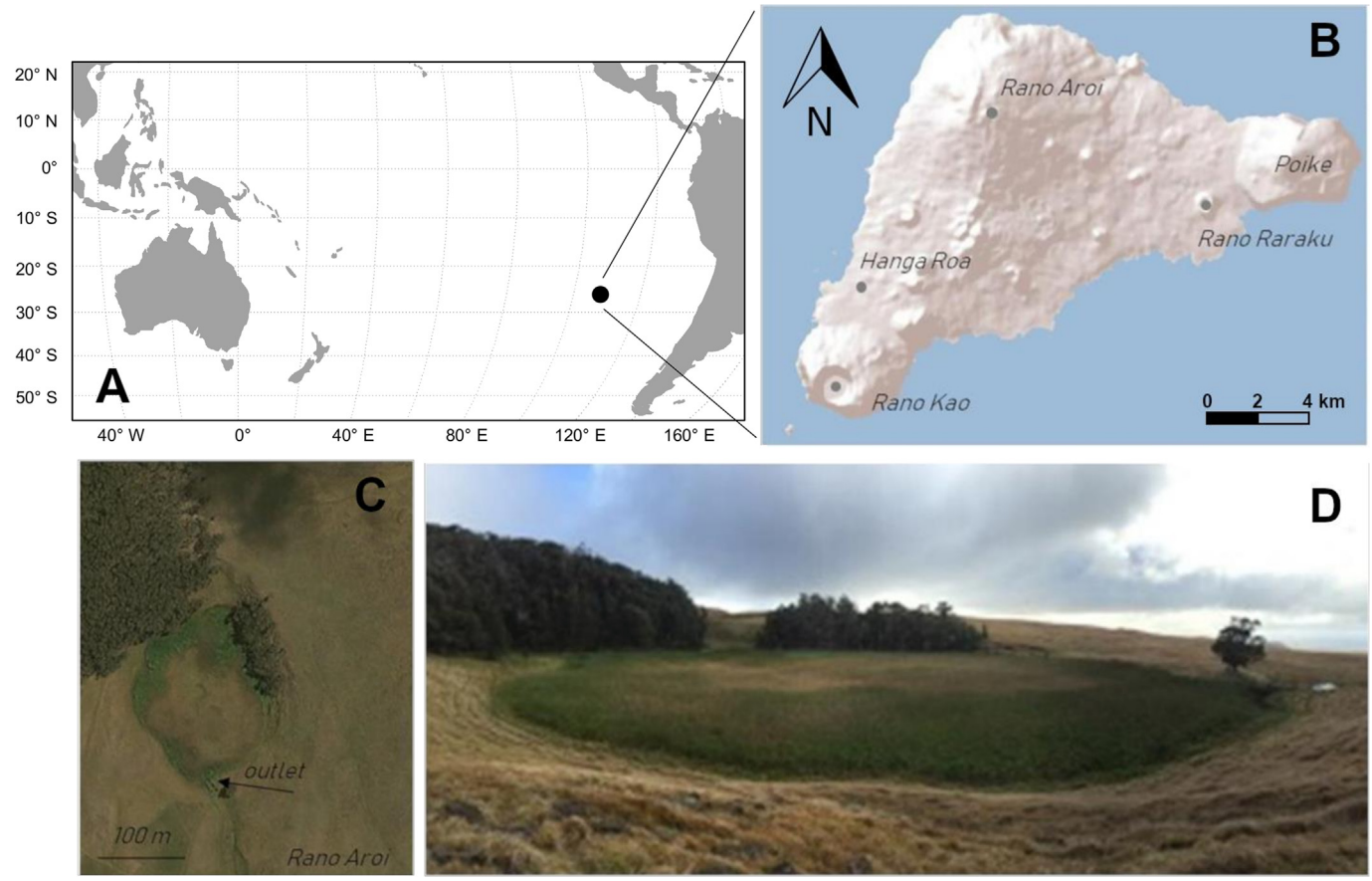

Fig. 1. (A) Geographic location of Rapa Nui; (B) Map of Rapa Nui showing the location of the three main water bodies; (C, D) aerial and lateral view of the Rano Aroi fen. The white dot in (C) marks the location where core LTS-AROI17-1A was drilled.

2. Materials and methods

2.1. Core and water samples

A set of peat cores were collected in September 2017 at −27.09434, −109.37392 in the Aroi wetland (Fig. 1). We collected three sections of peat approximately 290 cm long in total (LTS-AROI17-1A) and a parallel three-section core (LTS-AROI17-1B) using a Livingstone corer with a serrated edge to facilitate the coring of mixed wetland and peat sediments. Coring the wetland did not require a platform and we were able to stand on the wetland surface.

The Rano Aroi core sequence is dominated by fibrous peat including larger remains of roots particularly evident in the upper section of the core LTS-AROI17-1A (Fig. 2). A lighter ~15 cm band associated with a fibrous peat mixed with light clay sediments occurs between 15 and 32 cm. A second lighter band, likely due to a mineral sediment input, is present between 67 and 78 cm, although this lighter band is less evident from the image in Fig. 2. The dominance of fibrous peat throughout the core sequence is remarkably consistent, even despite an abrupt change in sedimentation indicated by the age-depth model at 110–115 cm (see below).

The core sections were sealed and transported to the LacCore Repository (University of Minnesota, USA) and stored at 4 °C until sub-sampling. In this study, we focus on intervals associated with human arrival represented by the uppermost ~130 cm of the sediment sequence spanning the last 2000 cal y BP. The core was sub-sampled at 1-cm vertical resolution for chemical analysis. The ~70 resulting contiguous wet samples were freeze-dried, hand milled, homogenized in a ceramic mortar and dry-sieved using a 2 mm nylon sieve. All the samples were stored at 4 °C until analysis.

In proximity to the artificial outlet located at the southern side of the swamp, we collected ~0.5 L of water to analyze the TE and REE composition of water leaving the wetland. Water samples were filtered in the field through 0.45 μm cellulose nitrate membranes (Whatman) using a polycarbonate system equipped with a manual vacuum pump. Membranes containing suspended particulate matter (SPM) were stored in plastic Petri dishes, while the filtered water was kept in 50 mL HDPE bottles. Sediment, water and SPM samples were stored at 4 °C until analysis.

2.2. Multi-elemental analysis

The determination of TE and REE in the sediment and SPM was carried out by acid digestion in a microwave oven, followed by inductively coupled plasma-mass spectrometry (ICP-MS) analysis. Approximately 200 mg of each sample was digested with a mixture of HNO_3, HCl and HF (6:2:1 mL, super purity grade acids, Romil), using an Ethos1 microwave oven (Milestone) and a temperature-controlled program specifically optimized for complete mineralization at temperatures up to 200 °C in pressurized Teflon vessels. The digests were appropriately diluted in ultra-pure water to fit the calibration range, randomized and analyzed by ICP-MS using an iCAP RQ (Thermo Scientific) instrument equipped with an ASX-560 autosampler (Teledyne Cetac Technologies), PFA cyclonic spray chamber at 2.7 °C, sapphire injector, quartz torch, Ni cones and 1550 W of plasma radio frequency power. The acquisition was

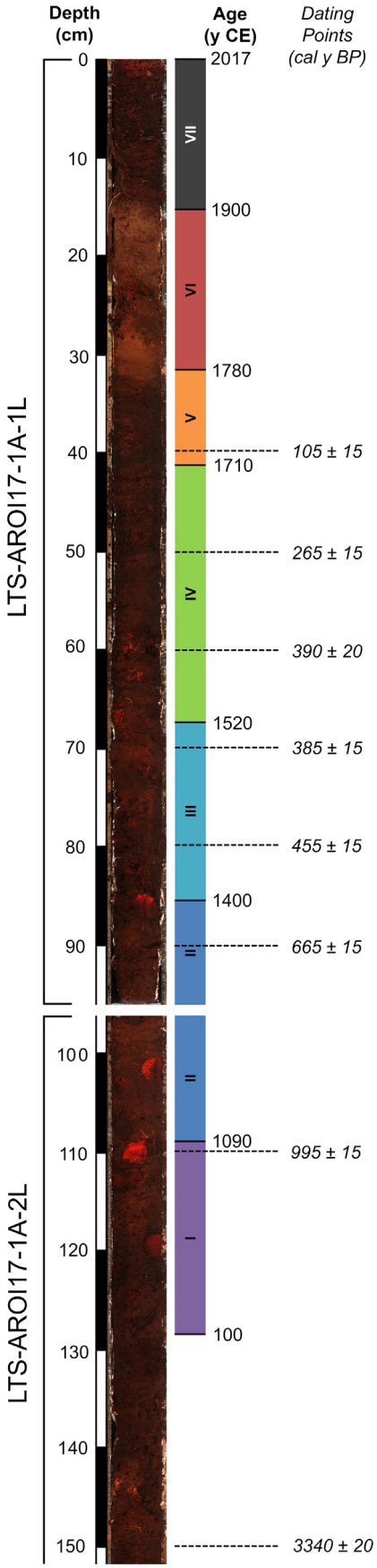

performed in kinetic energy discrimination – high matrix mode using He as the collision gas (4.3 mL min^{-1}). A total of 43 elements were monitored including: the TE of B, Na, Mg, Al, Si, P, K, Ca, Sc, Ti, V, Cr, Mn, Fe, Co, Ni, Cu, Ga, Ge, As, Se, Sr, Y, Mo, Cd, Ba, Pb, Th and U; and the REE of La, Ce, Pr,Nd, Sm, Eu, Gd, Tb, Dy, Ho, Er, Tm, Yb and Lu. All elements were acquired in triplicate and quantified by external calibration with standards prepared from the multi-elemental solutions IMS-101, IMS-102 and IMS-104 (Ultra-Scientific). These standards were prepared in ultrapure grade HNO_3 2% v/v using a combination of the certified multi-elemental solutions IMS-101, IMS-102 and IMS-104 (10 μg g^{-1}, Ultra Scientific) to span the range 0.02–200 ng g^{-1} (TE) or 0.002–20 ng g^{-1} (REE). On-line spikes of Rh at 1 ng g^{-1} was used as the internal standard. Accuracy was assessed by contextual mineralization and analysis of the certified reference materials NIMT/UOE/FM/001 (peat) and BCR-667 (estuarine sediment). The certified reference materials help evaluate the method accuracy for the different matrixes that are present in the mire. Despite the limited number of elements available in the certified materials, we obtained accuracies that deviate less than the 20% from the certified value.

Quantification of TE and REE in water was performed using an inductively coupled plasma - sector field mass spectrometer (ICP-SFMS model Element-XR, Thermo Scientific). Water samples were acidified with ultrapure grade HNO_3 (Romil) before the analysis. The quantification was carried out by external calibration as reported above. Method accuracy was assessed through the analysis of a certified reference material (TMRAIN95).

Total Organic Carbon in sediments (OC %) was determined through a Flash 2000 Thermo Scientific Elemental Analyzer (Krotz et al., 2016). A small amount of dry sample (~200 μg) was weighed, treated with HCl (1:1) and sealed into tin capsules, then introduced in the CHNO quartz reactor. The reactor temperature was 950 °C, while the column was held at 65 °C. Samples were analyzed in triplicate.

2.3. Depth-age chronology

Dating was performed at the National Ocean Sciences Accelerator Mass Spectrometry (NOSAMS) facility according to standard AMS protocols. Given that all the samples were classified as peat from lithological analysis, the acid-base-acid pretreatment was used to remove inorganic carbon and mobile organic acid phases (humic acids). Eleven accelerator mass-spectrometry ^{14}C ages were derived from plant materials (bulk peat) sampled throughout the three core sections (Table 2). The ^{14}C ages were converted to calibrated ages using the SHCal13 calibration curve (Hogg, 2013) and all radiocarbon ages were included in the depth-age model using Bayesian accumulation histories for deposits (BACON) software for modeling (Blaauw and Christeny, 2011) in R (R Core Team, 2019) (Fig. 3). Reservoir effects were assumed to be negligible due to the efficient CO_2 exchange with the atmosphere (the lake has a very high surface-to-volume ratio) and absence of significant dissolved carbon inputs from groundwater (the bedrock is volcanic).

2.4. Data elaboration

More than 20% of the samples had values below the detection limit for the TE including B, Ge, As, Se, Mo, Cd, Pb, Th and U, as well as the REE Tb, Ho, Tm and Lu. The elaborations were therefore carried out on a reduced dataset including: Al, Ba, Ca, Co, Cr, Cu, Fe,

Fig. 2. Images of the LTS-AROI17-1A core profile covering the last 2000 years. Dashed lines indicate the dating points and the numbered bars encompass sections (I-VII) that correspond to the clusters identified by statistical analysis.

Ga, K, Mg, Mn, Na, Ni, P, Sc, Si, Sr, Ti, V, Y and the remaining REE. Their distributions were checked for normality using the Shapiro-Wilk (SW) test. As only two elements have normal distributions (Ca and Sr), we applied a Box-Cox transformation to all distributions for consistency prior to further data elaboration. Multivariate data analyses were performed on the pooled dataset including TE, the sum of all REE (ΣREE, including all highly correlated elements with r > 0.91), the OC % and the sedimentation rate (23 variables overall), *previa* standardization, following the approach of Battistel et al. (2018). Hierarchical cluster analysis was applied to differentiate similar groups of samples within the core. Similarity between clusters is defined by their Euclidean distance where the results are grouped using the Ward method. The number of significant clusters was established by a visual interpretation of the scree plot (Fig. S2), the outcome of the Silhouette method, as well as paleoclimatic cross-interpretation. Principal component analysis (PCA) was used to reduce further the dataset to a few synthetic variables. The number of significant components was selected according to the Kaiser-Gutmann criterion. Further details on the adopted statistical approach are reported in the Supplementary Information. All statistical analyses were carried out using the stats pvstat packages for RStudio.

3. Results

All data collected in this research are available on the NOAA/WDS Paleoclimatology data repository at the link: https://www.ncdc.noaa.gov/paleo/study/33612.

3.1. Depth-age chronology

The depth-age model for the Rano Aroi record is presented in Fig. 3. Mean sedimentation rates from 1400 CE to present were >0.14 cm^{-2} y^{-1}, representing the highest sedimentation rates for the entire record. Sedimentation rates from 0 to 1400 CE were >0.03 cm^{-2} y^{-1}, significantly lower than in the upper sections. The depth-age chronology derived from radiocarbon-dated material from the Rano Aroi sediments in this study improves on uncertainties in chronologies reported in previous research (Fig. 3). We focus our analyses on the multi-elemental characterization of the last 2000 years to better understand climate, human and environmental interactions.

3.2. Major and trace elements

The basic statistics of elemental concentrations in the sediment and water samples are reported in Table 3. According to the Shapiro-Wilk test, all of the elemental distributions in the core are non-normal and positively skewed, with the exception of Ca and Sr. Most elemental levels are highly variable throughout the core, but characteristic trends and phases are clearly identifiable within the record with the support of cluster analysis and PCA. Based on the analysis reported in detail in the Supplemental Information, the dendrogram obtained from cluster analysis (Fig. 4A) and the PCA biplots (Fig. 4B and C) show the presence of seven main groups of samples that coincide with seven chronologically well-defined core sections (here named as I to VII). In the PCA ~85% of the total variance is explained by the first four and significant components, whose elemental loadings are reported in Table 4. The first component (PC1) explains ~45% of the total variance and is characterized by high negative loadings of lithogenic elements such as Al, Sc, V, Ti and a positive loading of the OC%. The second component (PC2) accounts for the ~20% of the total variance and is characterized by high positive loadings of redox-sensitive elements such as Mn, Co and Fe, and negative loadings of K, Cu and Na. The third component (PC3, 13.5% of the total variance) has high negative loadings of Sr and Ca. Although the fourth component (PC4) explains only 6.5% of the total variance, PC4 helps to better interpret the groups identified by cluster analysis, and therefore is also considered. This component is characterized by a high positive loading of Mg and negative loadings of Y, ΣREE and the accumulation rate.

The grouping of samples into core sections based on their elemental composition corresponds to distinctive temporal variations throughout the record (seven main phases I-VII possibly divided into sub-phases *a*-*b*), as outlined by the evolution of PCs represented in Fig. 5 and schematically summarized in Table 5. PC1 and the associated negative loading of AI and Ti and positive loading of OC% mainly track the contribution of lithogenic elements that were more significant during sub-phase III-*b* and phase VI. The dominance of PC1 coincides with lighter mineral units (see Fig. 2) and may be interpreted as an increase in the input deriving from mineral particles transported through hydric erosion. The progressive decrease of PC2 over the last 300 years marks a change in the dominance of redox-sensitive elements (positive loadings) in phase V to high mobility elements (negative loadings) in phase VII. PC3 is mainly characterized by negative loadings of the alkaline earth elements (Ca and Sr) and decreases in correspondence to phase III and in the earliest part of phase VI. Finally, PC4 substantially increases during phase VI. Since the negative loadings of Y, ΣREE and OC % are the main contributors to this interval, in conjunction with less terrestrial input (see PC1), this component may be indicative of the geochemical processes occurring within the Aroi wetland rather than contributions of partitioned exogenous material.

3.3. Rare earth elements

The basic statistics of REE in the Rano Aroi record are reported in Table 6. The REE concentrations substantially vary along the core with enrichment factors (reported in Table S1, for definitions see Shotyk, 1996) ranging between 0.10 and ~7, suggesting partitioning of these elements in the Aroi wetland. In all of the samples from phase II-*a* as well as in 3 samples of phase VI, Er, Yb and Eu were

Table 2
Summary of Conventional Radiocarbon Ages (CRA in y BP (i.e. before 1950 CE) for samples from the Rano Aroi peat/sediment cores.

Depth cm	Lab ID	Material dated	CRA in y BP (error)	Calibrated Age in y median (range)
40	161633	Bulk peat	105 (15)	65 (26–238)
50	161634	Bulk peat	265 (15)	292 (283–303)
60	161635	Bulk peat	390 (20)	393 (329–485)
70	161636	Bulk peat	385 (15)	381 (329–466)
80	161637	Bulk peat	455 (15)	494 (487–503)
90	161638	Bulk peat	665 (15)	606 (559–614)
110	161639	Bulk peat	995 (15)	854 (809–911)
150	161640	Bulk peat	3340 (20)	3522 (3481–3563)

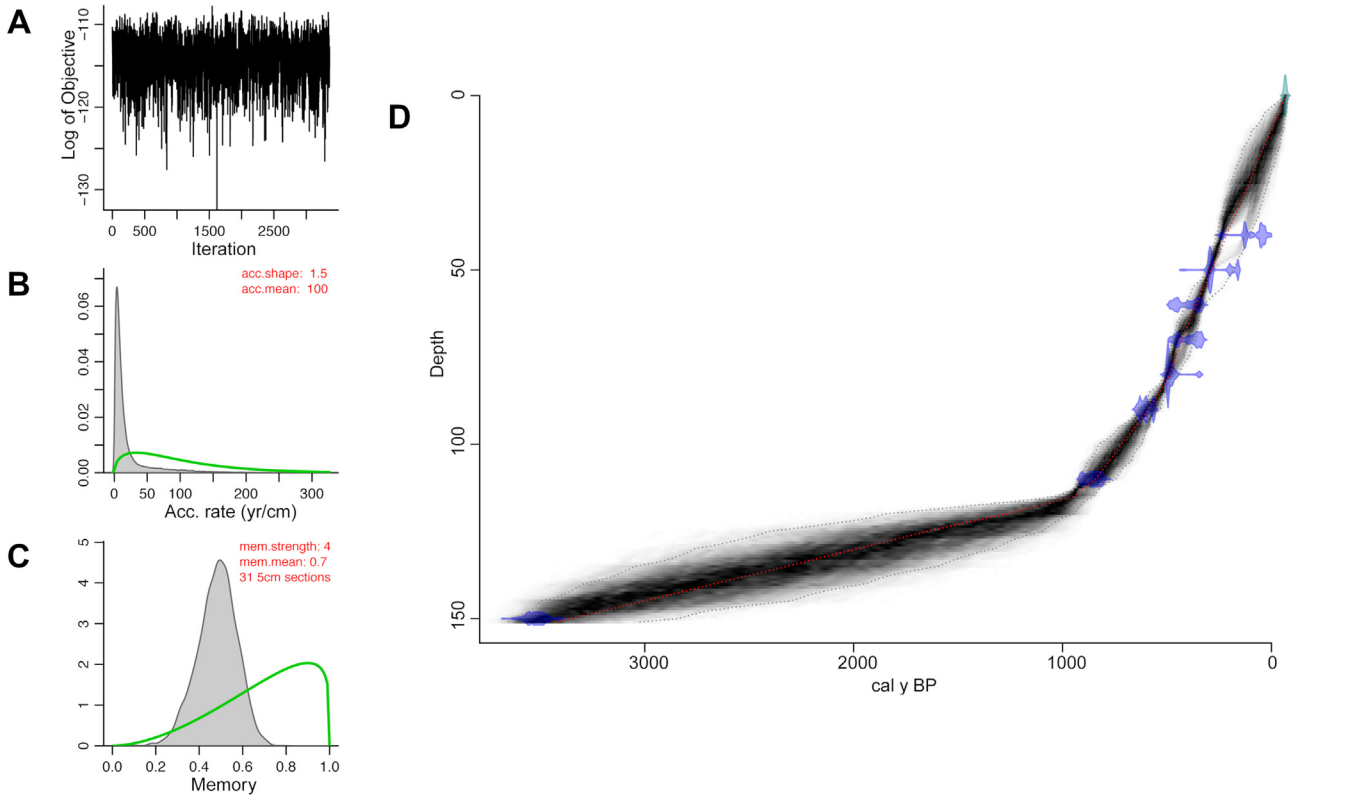

Fig. 3. Depth-age chronology based on ^{14}C ages reported in Table 2 (A) MCMC iterations showing stationary distribution; (B) prior (green curve) and posterior (grey histogram) distribution for the accumulation rate; (C) prior (green curve) and posterior (grey histogram) distribution for the memory; (D) Calibrated ^{14}C dates (transparent blue) and the depth-age model (darker greys indicate more likely calendar ages, grey stippled lines show 95% confidence intervals). (For interpretation of the references to color in this figure legend, the reader is referred to the Web version of this article.)

Table 3
Trace and major elements determined in the Aroi sedimentary record (mean, maximum and minimum values), water and suspended particulate matter (SPM) collected in proximity of the outlet (mean ± standard deviation). W statistics and p-values refer to the Shapiro-Wilk (SW) normality test. H_0: the null hypothesis of normal distribution is accepted vs. H_1: the null hypothesis is rejected. Missing values mark concentrations lower than their respective detection limits.

Element	Sediment						Water		SPM	
	mean	min	max	W	*p*-value	SW hyp				
Al (g kg^{-1})	2.2	0.3	17	0.512	<0.001	H_1	152 ± 15	µg L^{-1}	590 ± 60	µg L^{-1}
Ba (mg kg^{-1})	4.4	0.9	50	0.412	<0.001	H_1	2.3 ± 0.2	µg L^{-1}	0.5 ± 0.1	µg L^{-1}
Ca (mg kg^{-1})	240	5	600	0.981	0.430	H_0	2.0 ± 0.2	mg L^{-1}	52 ± 5	µg L^{-1}
Co (mg kg^{-1})	2.0	0.5	16	0.459	<0.001	H_1	730 ± 70	ng L^{-1}	0.5 ± 0.1	µg L^{-1}
Cr (mg kg^{-1})	4.3	0.7	40	0.440	<0.001	H_1	350 ± 35	ng L^{-1}	26 ± 2	µg L^{-1}
Cu (mg kg^{-1})	6.8	1.0	36	0.740	<0.001	H_1	2.2 ± 0.2	µg L^{-1}	11 ± 2	µg L^{-1}
Fe (g kg^{-1})	6.4	0.6	50	0.624	<0.001	H_1	700 ± 65	µg L^{-1}	1.9 ± 0.2	mg L^{-1}
Ga (mg kg^{-1})	2.6	0.1	34	0.357	<0.001	H_1			0.6 ± 0.1	µg L^{-1}
K (mg kg^{-1})	70	30	320	0.627	<0.001	H_1	0.76 ± 0.08	mg L^{-1}	103 ± 10	µg L^{-1}
Mg (g kg^{-1})	0.74	0.26	1.6	0.932	0.001	H_1	2.0 ± 0.2	mg L^{-1}	70 ± 7	µg L^{-1}
Mn (mg kg^{-1})	54	8	380	0.568	<0.001	H_1	31 ± 3	µg L-1	4.8 ± 0.5	µg L^{-1}
Na (mg kg^{-1})	150	47	500	0.750	<0.001	H_1	35 ± 4	mg L^{-1}	9.5 ± 1.0	µg L^{-1}
Ni (mg kg^{-1})	170	18	1300	0.621	<0.001	H_1	750 ± 80	ng L^{-1}	1.1 ± 0.1	µg L^{-1}
P (mg kg^{-1})	350	100	2000	0.538	<0.001	H_1				
Sc (mg kg^{-1})	0.7	0.1	6	0.530	<0.001	H_1				
Si (g kg^{-1})	6.8	0.4	77	0.401	<0.001	H_1				
Sr (µg kg^{-1})	28	3	54	0.978	0.310	H_0	27 ± 3	µg L^{-1}	1.1 ± 0.1	µg L^{-1}
Ti (g kg^{-1})	1.9	0.03	30	0.360	<0.001	H_1				
V (mg kg^{-1})	25	1	300	0.376	<0.001	H_1	700 ± 70	ng L^{-1}	6.2 ± 0.5	µg L^{-1}
Y (µg kg^{-1})	350	40	1200	0.832	<0.001	H_1				
OC %	50.1	29.8	68.6	0.754	<0.001	H_1				
ΣREE (mg kg^{-1})	2.4	0.4	12	0.614	<0.001	H_1	330 ± 40	ng L^{-1}	97 ± 10	ng L^{-1}

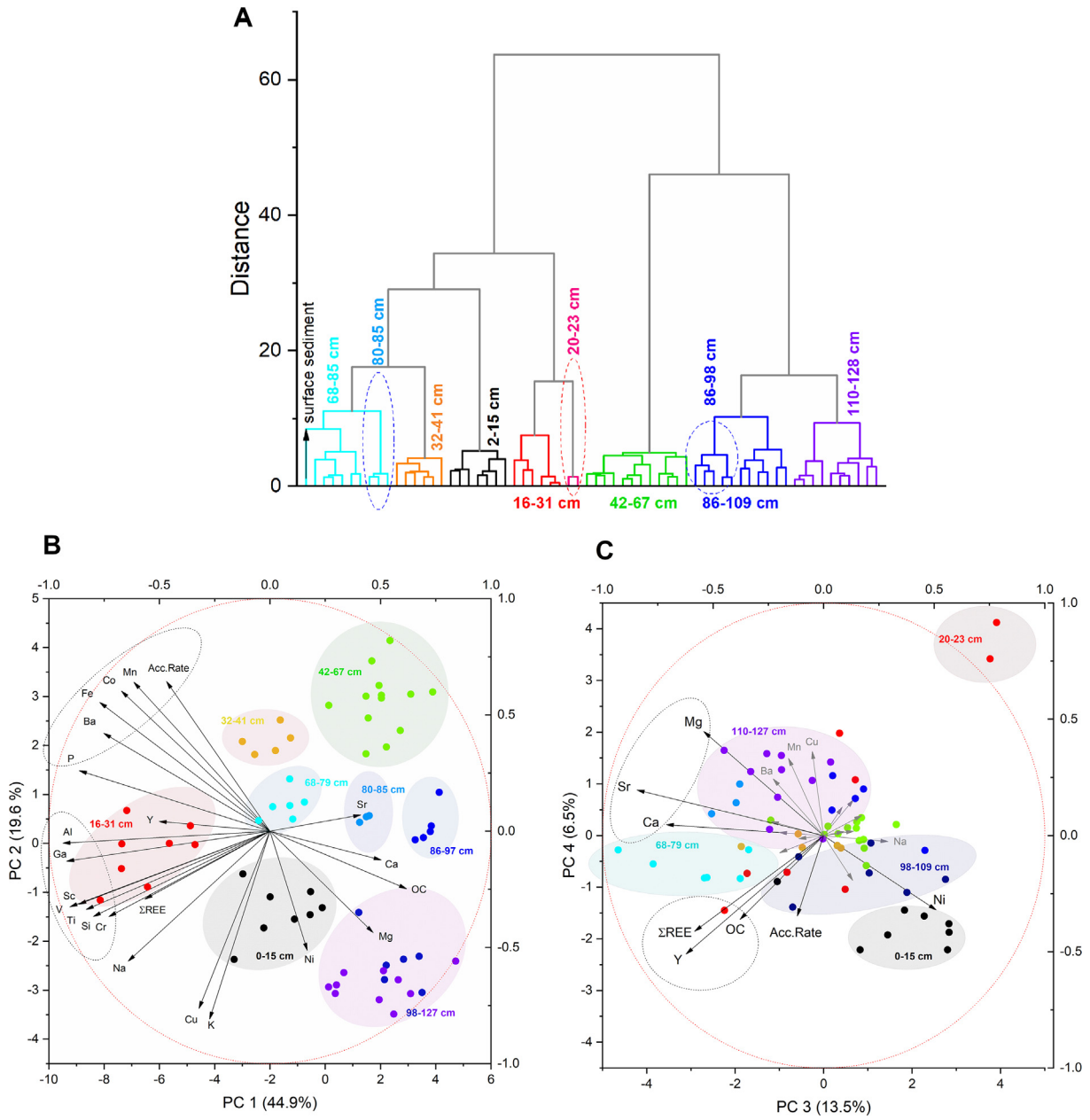

Fig. 4. (A) Dendrogram obtained by hierarchical cluster analysis using the Euclidean distance and Ward's method. Principal component bi-plot: PC1 *vs* PC2 (B) and PC3 *vs* PC4 (C). The color of the scores correspond to the color associated with the groups indicated in (A). (For interpretation of the references to color in this figure legend, the reader is referred to the Web version of this article.)

below their detection limits, while Ho, Lu, Tb and Tm concentrations were below the detection limits in more than the 50% of the samples. The mean concentrations of REE follows the typical Oddo-Harkins rule. Once the REE are normalized by chondrites they demonstrate enrichment in light REE (LREE) and are consistent with patterns previously observed in basaltic rocks from the three volcanoes of Rapa Nui (Margalef et al., 2014). The pattern of REE at Rano Aroi also correlates with the REE pattern observed in the upper crust reference (UCC; r = 0.998; *p*-value<10^{-5}), World Shale Average (WSA; r = 0.991; *p*-value<10^{-5}), North American Shale Composite (NASC; r = 0.998; *p*-value<10^{-5}) and Post-Archean Australian Shale (PAAS; r = 0.998, *p*-value<10^{-5}).

The fractionation between LREE (i.e. La, Pr, Nd, Sm) and HREE (i.e. from Gd to Yb) was evaluated through the $(La/Sm)_N$, $(Gd/Yb)_N$ and $(La/Yb)_N$ ratios normalized to UCC (as indicated by the subscript $_N$). We use La, Gd and Yb since many HREE are below their respective detection limits. The use of different reference standards (WSA, NASC or PAAS) do not significantly affect the calculated ratios (Table S2). As shown in Fig. 6 all of the samples from Rano Aroi provide $(Gd/Yb)_N$ values between 1 and 2.5, while $(La/Sm)_N$ varies between 0.30 and 1.80. Notably, only the samples from the deepest section of the core (phase I, violet dots) have $(La/Sm)_N$ values higher than the surrounding rocks (Margalef et al., 2014). In the water and SPM collected at the Rano Aroi outlet, $(La/Sm)_N$ ratios are 0.16 and 3.01, and $(Gd/Yb)_N$ ratios are 1.16 and 0.80, respectively, resulting in a more marked fractionation of $(La/Sm)_N$ compared to $(Gd/Yb)_N$. This occurrence is not unexpected, as LREE are generally less soluble than the other REE. The fractionation between water and SMP

Table 4
Loadings of the variables corresponding to the first four components of the PCA.

Element	PC 1	PC 2	PC 3	PC 4
Al	−0.937	−0.052	−0.199	−0.074
Ba	−0.753	0.421	−0.228	0.244
Ca	0.504	−0.123	−0.712	0.047
Co	−0.672	0.602	0.135	0.154
Cr	−0.729	−0.368	0.173	0.087
Cu	−0.321	−0.763	−0.051	0.362
Fe	−0.770	0.554	0.084	0.123
Ga	−0.920	−0.129	−0.200	0.013
K	−0.273	−0.809	0.136	0.019
Mg	0.467	−0.436	−0.542	0.447
Mn	−0.616	0.641	−0.159	0.332
Na	−0.641	−0.560	0.292	−0.026
Ni	0.169	−0.513	0.509	−0.320
P	−0.864	0.260	0.132	−0.193
Sc	−0.865	−0.314	−0.237	0.060
Si	−0.799	−0.368	0.093	0.017
Sr	0.411	0.070	−0.844	0.196
Ti	−0.832	−0.337	−0.165	0.125
V	−0.905	−0.326	−0.113	−0.14
Y	−0.502	0.042	−0.622	−0.510
OC %	0.618	−0.248	−0.378	−0.361
Acc. Rate	−0.468	0.644	−0.119	−0.346
ΣREE	−0.566	−0.292	−0.583	−0.412

is also confirmed by the ratio $(La/Yb)_N$ (0.33 and 2.03, respectively).

The potential effect of environmental redox conditions and/or dynamics involving the formation of organic complexes and/or leaching processes on REE fractionation was evaluated by calculating the Ce anomaly, as defined by Elderfield and Greaves (1982):

$$\delta Ce = \frac{3 \cdot Ce_N}{2 \cdot La_N + Nd_N} \quad (1)$$

In Rano Aroi peat samples, δCe ranges between 0.6 and 2.1, although higher values occur during phase VI-*a*. In contrast to the other REE, Ce anomalies in water and SPM were 0.96 and 1.1, respectively, suggesting a limited partitioning between such phases.

3.4. Elemental ratios

In order to investigate the in-peatland dynamics, key elements including Fe, Ca, K and P were normalized by Al or Ti (as molar ratios) and represented in Fig. 7. The K/Al ratio shows scarce variability during phase I, while the ratio markedly decreases between 1400 and 1520 CE and between 1710 and 1900 CE. The Ca/Ti ratio shows two main peaks between 1250 and 1440 CE and between 1520 and 1710 CE. The P/Al ratio contains peaks corresponding to 1090–1400 CE and to 1520–1710 CE, and minima at 1400–1520 CE and 1800–1900 CE. The values of Fe/Al vary between 1.2 and 3.0, close to the composition of the surrounding rocks (1.0–1.5, Margalef et al., 2014). A marked enrichment of Fe/Al values occurs between 1520 and 1790 CE and weaker peaks are observed at 1200–1400 CE and 1900 CE-present. The Mn/Al ratio (not shown) follows the same trend as Fe/Al (r = 0.825). The average Mn/Fe of ~0.0058 observed in the peat is close to that of SPM (Mn/Fe = 0.0025), but lower than the ratio in the water (Mn/Fe = 0.044). During the last two millennia, Mn/Fe ratios oscillated from ~0.002 to ~0.018, reaching maximum values between 1090 and 1520 CE.

4. Discussion

4.1. Paleogeochemical significance of elemental proxies

Four main components were identified in the PCA analysis that

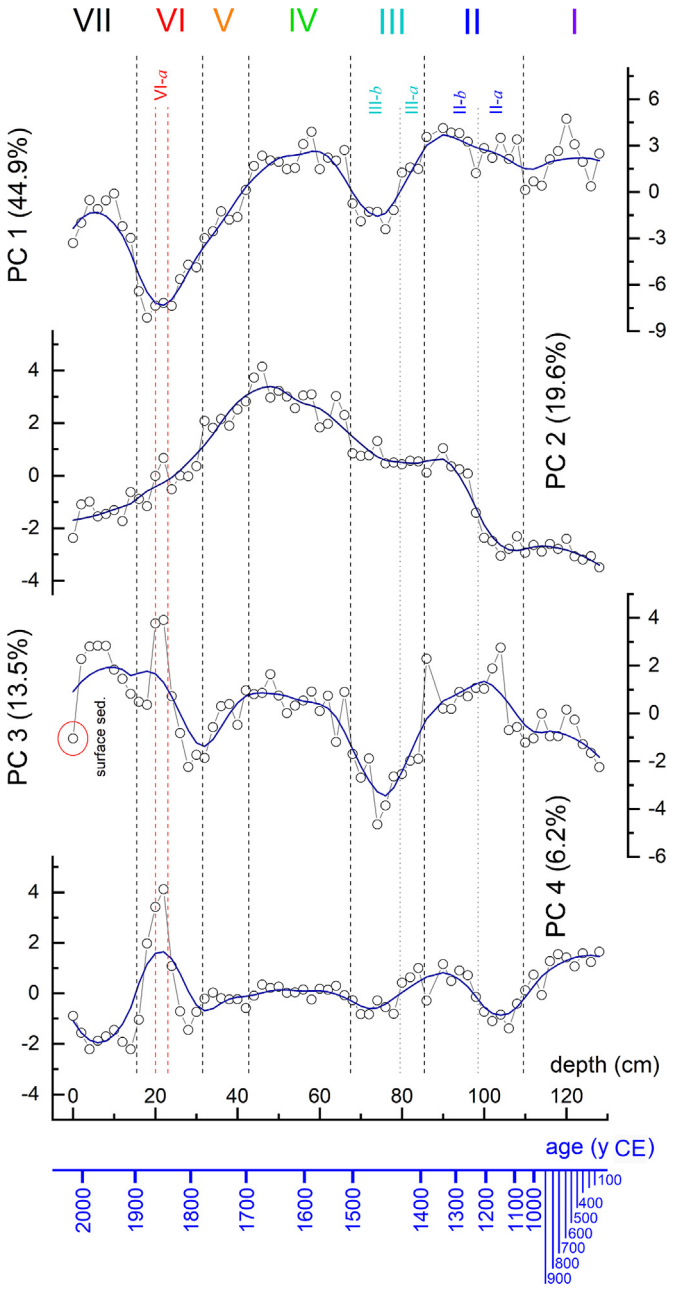

Fig. 5. Temporal evolution of the principal components along the Rano Aroi record. Colored numbers refer to the phases indicated in Fig. 4, reported in Table 5 and discussed in the text.

Table 5
Summary of the qualitative trends derived from the principal component analysis in the Rano Aroi records sections and corresponding chronological phases. ▲ positive, ▼ negative, - not significant.

	Phase	Depth (cm)	Age (years CE)	PC1	PC2	PC3	PC4
●	I	110–128	1st century – 1090	▲	▼	-	▲
●	II-a	98–109	1090–1200	▲	▼	▲	-
●	II-b	86-98 c	1200–1400	▲	-	-	▲
●	III-a	80–85	1400–1440	▲	-	▼	-
●	III-b	68–79	1440–1520	-	-	▼	-
●	IV	42–67	1520–1710	▲	▲	-	-
●	V	32–41	1710–1790	-	▲	-	-
●	VI-a	16–31	1710-1780 E	▼	-	-	-
●	VI-b	20-23 c	1840–1865	▼	-	▲	▲
●	VII	2-15 c	1865-Present	-	▼	▲	▼

Table 6
REE concentrations and ratios normalized by UCC in the Aroi sedimentary record, water and suspended particulate matter (SPM) collected in proximity of the outlet (mean, maximum and minimum values). W statistics and p-values refer to the Shapiro-Wilk (SW) normality test. H_0: the null hypothesis of normal distribution is accepted vs. H_1: the null hypothesis is rejected. n.d. not determined.

REE	Sediment							Unit	Water	SPM
	Unit	mean	min	max	W	*p*-value	SW hyp			
La	μg kg^{-1}	440	62	1535	0.864	<0.001	H_1	ng L^{-1}	40.4	22.1
Ce	"	993	183	6800	0.663	<0.001	H_1	"	110.3	41.7
Pr	"	93	18	375	0.763	<0.001	H_1	"	15.8	5.6
Nd	"	420	70	1700	0.764	<0.001	H_1	"	58.8	10.8
Sm	"	96	13	420	0.731	<0.001	H_1	"	37.9	1.1
Eu	"	29	4	120	0.744	<0.001	H_1	"	5.8	1.8
Gd	"	98	6	370	0.759	<0.001	H_1	"	18.2	1.1
Tb	"	13	5	56	n.d.	n.d.	n.d.	"	2.9	1.8
Dy	"	90	6	340	0.760	<0.001	H_1	"	18.2	2.3
Ho	"	14	0.3	60	n.d	n.d.	n.d.	"	3.6	2.0
Er	"	44	7	175	0.779	<0.001	H_1	"	10.2	2.0
Tm	"	–	–	–	n.d.	n.d.	n.d.	"	10.5	1.5
Yb	"	39	6	162	0.775	<0.001	H_1	"	9.1	0.8
Lu	"	6	5	19	n.d.	n.d.	n.d.	"	1.5	1.6
δCe		0.94	0.66	2.10	0.650	<0.001	H_1		0.95	1.13
$(La/Yb)_N$		0.87	0.33	3.62	0.723	<0.001	H_1		0.33	2.03
$(Gd/Yb)_N$		1.50	1.02	2.50	0.939	0.005	H_1		1.16	0.80
$(La/Sm)_N$		0.73	0.32	1.81	0.836	<0.001	H_1		0.16	3.01

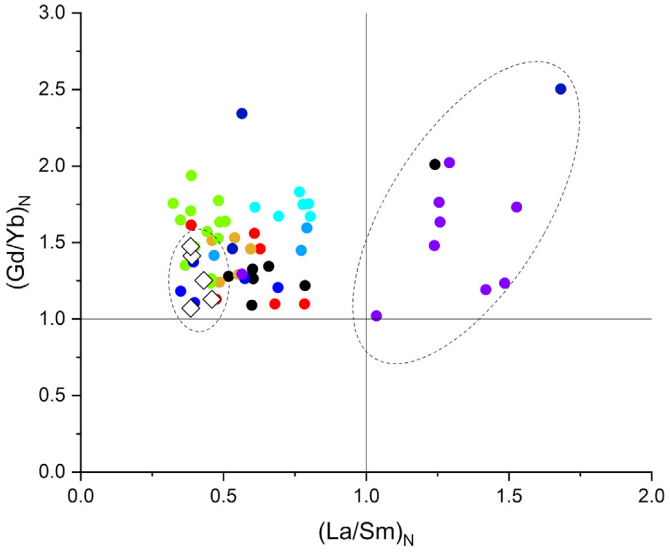

Fig. 6. $(Gd/Yb)_N$ plotted *vs* $(La/Sm)_N$. Peat samples at different depths are colored dots corresponding to the scale used for indicating groups in Figs. 4 and 5. The composition of the surrounding rocks (Margalef et al., 2014) is reported as empty diamonds.

enclose elements with similar quantitative trends within the Rano Aroi record, likely controlled by common geochemical processes in the mire, into a few variables representative of those processes. While the PCs capture trends in the *absolute* concentration of elements, elemental ratios (and similarly δCe) track the quantitative evolution of elements *relative* to other elements. The result is that all these proxies are representative of different (although multiple and interconnected) paleoclimatic processes. Fig. 7 provides an integrated graphical overview of these proxies showing the complexity of the geochemical evolution of Rano Aroi over the past 2000 years.

PC1 dominates the variability of Rano Aroi multi-elemental record overall. This PC is characterized by highly negative loadings of lithogenic elements including Al, Ti, Sc and V, and a positive loading of the OC %. As reported by Margalef et al. (2014), in Rano Aroi such elements are associated with primary mineral particles originating from the degradation of volcanic rocks and pedogenetic processes in the catchment basin, reaching the mire through aeolian transport and/or colluvium and input from groundwater. Aluminum and Ti have particularly low mobility, remain stable in the peat archive (Le Roux et al., 2006; Muller, 2006; Muller et al., 2008) and resist chemical weathering (Biester et al., 2012; Shotyk, 1996). The inverse association with the OC % in PC1 shows that the influx of exogenous lithogenic materials and vegetation within the mire are strongly coupled in an evolution which is not directly captured by the OC % alone (see Fig. 7). A similar association of elements coupled to the organic chemistry at Rano Aroi was also found by Margalef et al. (2014) over the last 70000 years, supporting a link between their temporal evolution and changes in the precipitation regimes. Baseline conditions in the Rano Aroi mire were characterized by regular water supply but limited detritic input due to the well-developed soils and dominance of C3 plants (Margalef et al., 2013), whereas drier climate shifted vegetation towards C4 plants, reduced pedogenesis, increased erosion and exacerbated lithogenic inputs trough aeolian transport (Margalef et al., 2014). At this level, distinguishing the aeolian vs. hydric origin of mineral particles represented by PC1 is still challenging, but water availability is also expected to affect the dynamics of leachable elements, particularly K and Na, which do not contribute to PC1. An enrichment (depletion) of K with respect to Al (or Ti) may be ascribed to a poorly (highly) leached mineral source and thus indicates the prevalence of physical (chemical) weathering, as shown in lacustrine sediments (Arnaud et al., 2016). Given that PC1 is more representative of absolute lithogenic inputs while K/Al is more linked to the relative leaching of their constituents, the coherent temporal evolution of these two proxies observed in our record (see Fig. 7) suggests a major role of hydric erosion (accompanied by chemical weathering) in the transport of lithogenic materials towards the mire during the (negative) peak phases of PC1, thus identified as flood events during wetter climatic conditions.

PC2 represents a different and complementary process, and is characterized by high positive loadings of Mn, Co and Fe, and negative loadings of K, Cu and Na. Manganese and Fe in particular can be transported into the mire as components of lithogenic particles, but are also subject to redox-dependent internal mobility and accumulation processes. The potential of such elements as proxies of specific exogenous mineral fractions or endogenous redox conditions depends on the characteristics of the application

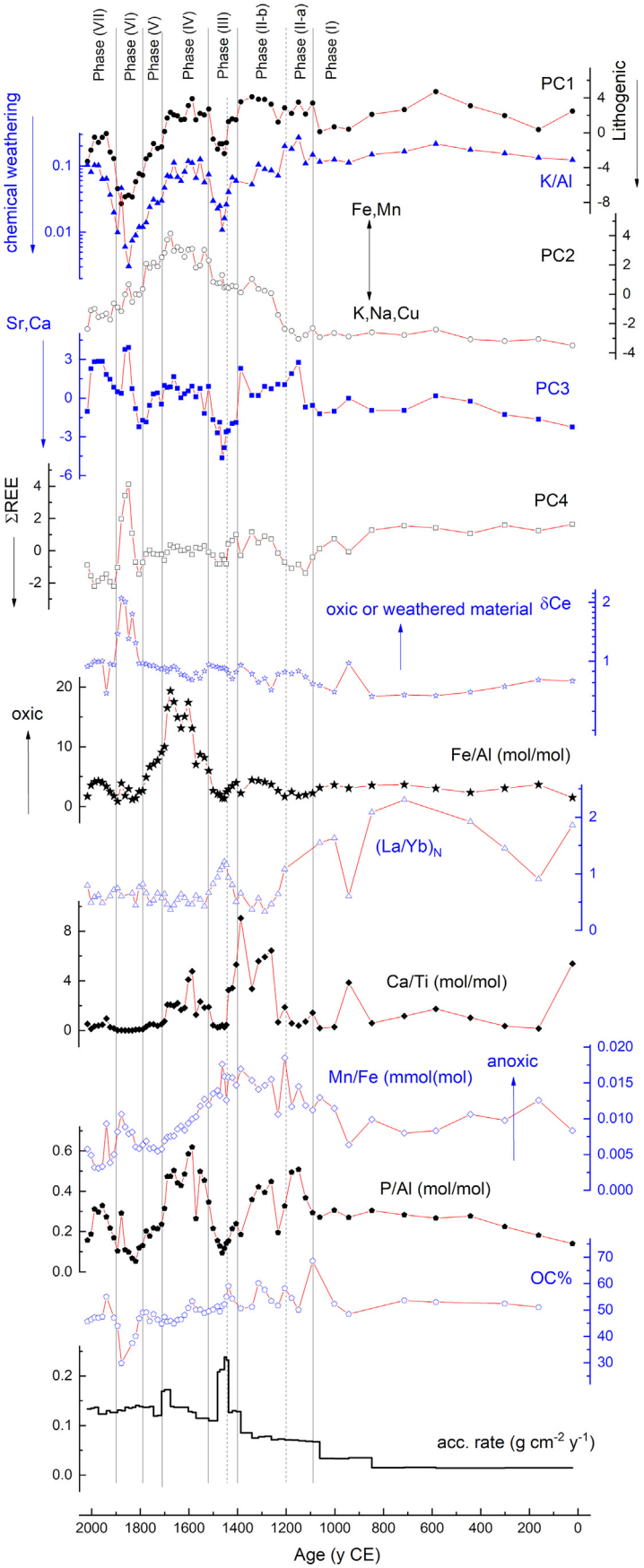

Fig. 7. Rano Aroi record of the environmental and climatic proxies discussed in this paper: principal components trends (PC1-PC4), weathering dynamics (K/Al); transport and deposition $(La/Yb)_N$, Ca/Ti; redox conditions (δCe, Mn/Fe and Fe/Al); P/Al, OC% and accumulation rate.

site and the period. Margaref et al. (2014) reported that between 70000 and 10000 cal y BP the level of Fe and Mn in Rano Aroi associate with Ba, Ti and Zr. The authors ascribed this combination to coarser mineral particles transported into the mire by intense runoff events, while considered redox effects not significant. Our findings suggest that during the last 2000 years PC2 is primarily representative of changes in the redox state of the system, specifically the onset of strongly oxic conditions, and only secondarily affected by lithogenic input during specific phases. The link amongst Fe, Mn and redox changes in peat systems is well known. Decomposition of organic matter is the product of contrasting mineralization and humification processes determined by the peat redox conditions that are, in turn, controlled by changes in the water table (Beer et al., 2008; Chesworth et al., 2006). In this view, peat decomposition may be affected by climatic and hydrological changes as mineralization is promoted under drier-oxic conditions with a lower water table, whereas wetter-anoxic conditions favor humification. Redox-sensitive elements such as Fe and Mn reflect these changes because their reduced forms Mn(II) and Fe(II) are more soluble than the oxidized forms Mn(IV) and Fe(III). Therefore, Mn and Fe tend to be depleted (enriched) in the peat under anoxic (oxic) conditions (Chesworth et al., 2006; Damman, A.W.H.; Tolonen, K.; Sallantaus, 1992). The fidelity of this relationship and the use of Fe and Mn as paleo-redox proxies might be complicated by at least two factors. Firstly, undisturbed peat systems are typically layered in an upper aerated level (acrotelm) and a lower anaerobic level (catotelm), so that both oxic and anoxic conditions co-exist. An upward movement of Fe(II) (and Mn(II)) from the catotelm to the upper aerated acrotelm, followed by the precipitation of Fe(III) (and Mn(IV)) oxides may lead to internal enrichment of the elements. Secondly, mineralization and/or humification may not be contemporary with the peat formation, but rather may be a secondary effect of older peat decomposition (Borgmark and Schoning, 2006), resulting into post-depositional re-distribution of Fe and Mn. In practice, these confounding processes limit Fe and Mn to be reliable proxies of extreme paleoredox conditions only. For instance, considerable Fe enrichment can track episodic droughts that intensely affect the saturation of the peatland (Margalef et al., 2013; Shotyk, 1988). Moreover, although both Fe and Mn are redox-sensitive elements, Mn is reduced more quickly than Fe. The corresponding Fe and Mn oxidized/reduced forms have different solubilities, mobilities and distributions at the water-sediment interface. As a result, the Mn/Fe ratio decreases in strongly anoxic peatland environments (Schittek et al., 2016). The synchronous changes shown by PC2 and Fe/Al in the Rano Aroi record (Fig. 7) suggest they are both proxies of strongly oxic conditions, marked by a distinctive coeval maximum. Still, the smoother variation of PC2 compared to Fe/Al suggests that high lithogenic inflows (PC1) and corresponding Fe, Mn from primary minerals may have contributed to PC2 during the phases adjacent to the maximum of Fe/Al ratio. The asynchronous maximum of Mn/Fe signal support distinct paleoclimatic influences for such proxy likely more indicative of anoxic than mild/oxic conditions.

The transition of oxic-anoxic environments in wetlands can also potentially be inferred by δCe (Davranche et al., 2017) since an increase in Ce concentrations in sediments is typically observed in oxic conditions, as Ce(III) is oxidized to the less soluble form Ce(IV). Positive anomalies of Ce can be correlated with enrichment of Mn(IV)-(oxyhydr)oxide minerals because oxidation of and subsequent adsorption of Ce preferentially occurs on their surface, but this association is not observed in the Rano Aroi record. However, the interpretation of the δCe signal is affected by other factors such as the differential leaching of the parent rocks as well as variations in the solubility of Ce ions when surfactants are present in the water body. In the Rano Aroi record, δCe presents a distinctive peak asynchronous with Fe/Al evolution, thus being not representative of endogenous oxic conditions. It is more likely that the Ce anomaly derives from two (eventually co-occurring) processes: 1) a depletion in relatively more soluble REE, other than Ce, associated with a chemically weathered source transported by hydrological processes; and/or 2) an increased input of particles from runoff, enriched in Ce by previous oxidizing conditions in the catchment basin. The concomitant intense chemical weathering marked by K/Al and drop in the absolute levels of all REE (from PC4) despite a generally intense lithogenic input (PC1) supports the first process as the major candidate for the anomaly in our record.

PC3 traces the behavior of Ca and Sr. Calcium is a typical major component of peat ashes. This element can be transported into the mire in conjunction with soil particles containing primary minerals, but its high mobility suggests that dissolution from Ca-bearing minerals may also be a major source of this element in the peat (Shotyk et al., 2002). The behavior of PC3 in the Rano Aroi record (Fig. 7) is characterized by moderate variations, with relative minima partially coeval with PC1 and K/Al. This evolution suggests a geochemistry of Ca mostly dominated by endogenous processes, with occasional spikes of exogenous material in association to events of high lithogenic input trough hydric erosion (see PC1 and K/Al). The internal recycling and mobility of Ca in fens is mainly controlled by combined changes in the redox-pH state. A shift from oxic-acidic to anaerobic−less acidic conditions, as typically occurs from the acrotelm to the catotelm, may drive the system towards formation of authigenic carbonate crystals, or in general an increase in Ca concentration with depth (Chesworth et al., 2006; Franzén, 2006; Glaser et al., 2006). In the anoxic environment, Ca can be incorporated into humic complexes together with reduced forms of Fe and Mg. In Rano Aroi, these processes and the corresponding rise in pH in the catotelm are expected to be generally limited or slow because the volcanic substrate would provide relatively low inputs of Ca regardless of climatic conditions. This also suggests a minor role of Ca in controlling the overall geochemistry of the mire, differently than on carbonatic substrates (Chesworth et al., 2006; Margalef et al., 2014). Conversely, a relative accumulation of Ca in the uppermost peat due to a combination of a constant pH profile and intensive uptake and recycling by plants into the organic substrate could become dominant in bogs (Biester et al., 2012). In dry conditions, this endogenous process may be exacerbated by lowering of the water table and intensified mineralization (Margalef et al., 2014). The Ca/Ti ratio can account for these phenomena (Schittek et al., 2016) more specifically than the absolute level of Ca as in PC3. In our record we observe two characteristic periods of high of Ca/Ti, both corresponding to low exogenous input, but one occurred under highly anoxic conditions (see Mn/Fe), while the other occurred during highly oxic conditions (see Fe/Al). This divergence suggests that relative high values of Ca/Ti ratio could indicate two different processes leading to selective accumulation of Ca in the Rano Aroi mire. One is consistent with high water levels and stratification of the water table, with anoxic catotelm; the other is compatible with low levels of the water table, oxic conditions, intense uptake, recycling and subsequent mineralization of Ca driven by vegetational changes. The integrative interpretation of multiple proxies helps in discriminating these two processes phase-by-phase along the record.

PC4 is a variable mostly characterized by the positive loading of Mg and negative loadings of Y, ΣREE and the accumulation rate. The temporal variability of this component is characterized by a single intense peak (Fig. 7), occurring in a period of high lithogenic input, and corresponds to events of highly positive δCe and depletion in Ca, Sr (PC3). Overall, these associations suggest PC4 mostly serves as a proxy for selective leaching of REE other than Ce under mildly

oxic or sub-oxic conditions (see Mn/Fe).

Phosphorous is fundamental in many metabolic processes and is often the limiting factor for primary productivity. In aquatic environments, P is released through the re-mineralization of organic matter, is measured for total level (TP), and can function as a proxy for paleoproductivity in lacustrine systems (Tribovillard et al., 2006). In mires, the interpretation of P (or P/Al) signals is more challenging. The main source of P is from groundwater supply as atmospheric deposition is considered negligible where local anthropic sources are excluded (Koerselman, W. Verhoeven, 1992; Tipping et al., 2014). This groundwater supply makes the overall input of P in fens considerably higher than in bogs, but higher mineralization (associated with the lower pH) in the latter may re-equilibrate site-specific levels of P. Redox conditions may also affect mineralization, so that despite having potentially higher levels of P, fens may exhibit reduced availability compared with bogs due to increased geochemical sorption of mineralized P (Bridgham et al., 1998). In particular, the availability of Mn and Fe can promote P sorption on insoluble oxyhydroxides, favoring the precipitation of P and limiting its bioavailability. The latter process explains the clear spike of P/Al associated with the most dry/oxic conditions observed in our record (see Fe/Al in Fig. 7). Conversely, intense primary production can lead to release of P through humification. Overall, the specific mechanisms that control the recycling and bioavailability of P in peatlands are still poorly understood (Kellogg and Bridgham, 2003). The resulting role of P as potential limiting nutrient for primary production is observed in some cases (Bridgham et al., 1996; Chapin, 1998; Bedford et al., 1999) but is not an important factor in other studies (Koerselman, W. Verhoeven, 1992). Despite these differences, the paleo-variability of P in mires may represent changes in the plant community (Zhao et al., 2007), that are possibly induced by water table instability (Hughes et al., 2000).

4.2. Reconstruction of the Rano Aroi environment over the last 2000 years

Characterization and multi-variate analysis of the Rano Aroi peat core elements over time indicate seven main phases in the temporal evolution of the local geochemistry over the last 2000 years (Table 5). The entire set of proxies including the PCs, diagnostic elemental ratios, δCe, OC% and the sediment accumulation rate (Fig. 7), in association with other geochemical and palynologic proxies from previous research, and regional climate reconstructions (Fig. 8), help decipher the biogeochemical processes underlying the environmental changes at Rano Aroi as discussed phase-by-phase in the following paragraphs.

4.2.1. Phase I (1st century-1090 CE)

Phase I is characterized by a low accumulation rate (0.01–0.03 g cm^{-2} y^{-1}) that provides centennial scale resolution. The high values of K/Al ratio and PC1 in this phase suggest a minimal hydric erosion, leading to low input of lithogenic elements (i.e. Ti, Al, Sc, Ga, V, Cr), and correspondingly limited chemical weathering. Compatibly with the results from Margalef et al. (2014), where the majority of mineral grains in the upper section of their AROI 06 01 core were quite small (10–20 μm), we argue that the lithogenic input to the wetland during this period may be mainly ascribed to aeolian transport from distant areas of the island. PC1 also coincides with a marked enrichment in LREE, as indicated by high $(La/Yb)_N$ (~2.0–2.5) and $(La/Sm)_N$ (~1.0–1.8) (Figs. 6 and 7). Although it is not possible to exclude that $(La/Yb)_N$ in this phase reflects the specific REE pattern of dust source areas different form Rano Aroi, a small size distribution is consistent with a slower deposition rate that promotes partitioning between HREE and LREE during transport, resulting in a high $(La/Yb)_N$ (Zhang et al., 2013). Iron and Mn concentrations are not particularly high during this phase and Fe/Al is only weakly enriched with respect to the surrounding rocks (Fig. 7). This combination suggests that the mire was subject to only mild anoxic conditions and is further supported by relatively high Mn/Fe and low δCe values. The state of Rano Aroi during phase I corresponds to the baseline status of the mire according to Margalef et al. (2013), defined by long-term stability of the water table near the surface.

All of these indications point to moderately dry to mesic conditions. Although the age model and the temporal resolution in phase I are insufficient to support a detailed interpretation, the record does not show evidence of spikes or trends during this

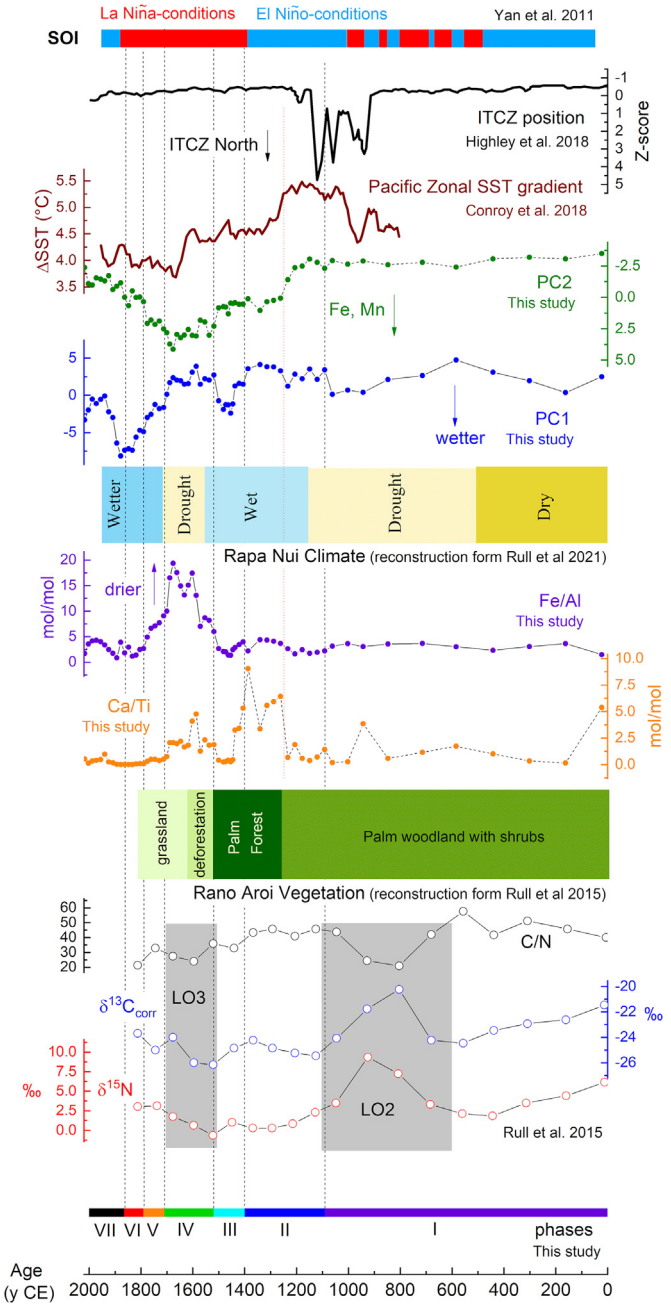

Fig. 8. Summary of the key paleogeochemical trends derived from trace elements in Rano Aroi over the last 2000 years, compared to previous local geochemical/vegetational and regional climate reconstructions.

period. This reconstruction is consistent with findings by Rull et al. (2015), who reported stable vegetation at Rano Aroi, comprised of palm woodland with underlying shrubs. The regional climate in Eastern Polynesia was consistently warm and dry during phase I (Nunn, 2007), possibly due to a stable position of the intertropical convergence zone (ITCZ) (Higley et al., 2018). A drought was previously suggested to have occurred between ~600 and ~1000 CE based on the presence of desiccation units in the Rano Raraku sediment archive (Cañellas-Boltà et al., 2013) and anomalies in $\delta^{13}C$, $\delta^{15}N$ and TN in Rano Aroi (Rull et al., 2015), as shown in Fig. 8. With the support of palynologic evidence, Rull et al. (2015) defined this period as a landscape opening, characterized by a shift from palm-dominated to grassland-dominated vegetation. This shift was considered as a sign of the Medieval Climate Anomaly (MCA) that is primarily observed in northern hemisphere archives and which is often placed between 700 and 1300 CE in archives across the globe (Conroy et al., 2010; Nunn et al., 2007; Yan et al., 2011). In the central tropical Pacific the MCA has been associated with a northward displacement of the ITCZ, stronger zonal sea surface temperature gradients and weakening of the South Pacific Convergence Zone (SPCZ) relative to the previous period, as well as with a general dominance of El Niño (Conroy et al., 2010; Higley et al., 2018; Yan et al., 2011). Such combinations would have reduced the moisture carried by the westerlies directed towards Rapa Nui (Margalef et al., 2014). However, these changes in major circulation patters and Rano Aroi geochemical records do not appear to be synchronous (Fig. 8). Within the limits of our temporal resolution, we do not observe a clear anomaly in geochemical signals from Rano Aroi corresponding to the onset of MCA. All of the above studies indicate phase I (and back to the last 30000 years; Flenley and King, 1984) as an overall stable warm-dry period. We can conclude that compatibly to the hypothesis of a limited influence of ENSO on Rapa Nui's climate and the resilience of the Rano Aroi area, the MCA anomaly was weak at most in the mire, insufficient to impact the geochemistry of the mire either way.

There is limited if any evidence for anthropogenic impacts at Rano Aroi during phase I. The majority of paleoenvironmental records from Rapa Nui indicate that human settlement in Rapa Nui occurred from 800 to 1200 CE (most likely in phase II). Rull (2021) assessed the hypothesis of an earlier colonization of Rapa Nui based on indications of forest clearing events, fires and exogenous pollen from Rano Kao and Rano Raraku records, yet human occupation of Rano Aroi would have occurred later than lowland sites. Within the limits of our low temporal resolution in this phase, effects of any earlier colonization, such as abrupt increases of non-chemically weathered lithogenic inputs due to forest cleaning and associated soils erosion, are not evident in data from the Rano Aroi peat sequence.

4.2.2. Phase II (1090–1400 CE)

Phase II consists of two distinct sub-phases between 1090 and 1200 CE (II-a) and 1200–1400 CE (II-b). Although both sub-phases are characterized by a decrease in Ca concentrations (PC3), Ca/Ti indicates a marked enrichment of Ca with respect to lithogenic elements from ~1250 CE to ~1440 CE, while the accumulation rate does not markedly change. Schittek et al. (2016) reported an enrichment of Ca relative to Ti in the same period in wetland sediments from the Andes, and interpreted this enrichment as due to the presence of shallow open water on the peatland surface. Ise et al. (2008) and Muller et al. (2008) ascribed enrichments in Ca to peat decomposition during drought phases. However, other indicators seem to contrast with this interpretation of droughts in our record during phase II. The K/Al ratio decreases from sub-phase II-*a* to sub-phase II-*b* suggesting a slight increase of chemical weathering despite lithogenic inputs remained substantially low (PC1). The Mn/Fe ratio indicates anoxic conditions that contrast with peat mineralization during drought phases. Iron and Mn concentration markedly increase from 1200 CE to 1400 CE (see PC2) in conjunction with a slight enrichment in Fe/Al. Since coarser particles could be more enriched in Mn and Fe (Margalef et al., 2014), this increase in absolute levels of Mn and Fe may be ascribed to a more local mineral source, and perhaps reflects a more relevant surface runoff versus previously dominant aeolian transport. However, as anticipated above, these processes are likely secondary in the overall dynamics of PC2 within our record. The lower $(La/Yb)_N$ values, closer to soil and rock composition, supports the hypothesis of a more local and less partitioned source. On the other hand, Ca enrichment may be explained by assuming that the transition to wetter conditions in the mire may have induced the bio-cycling of older Ca by plants. The stratification of the water table with increasingly anoxic conditions (and possible decrease of pH) during phase II would have further favored the authigenic accumulation of Ca in the catotelm, resulting in increased Ca/Ti while the mire was still experiencing reduced lithogenic inputs. Overall, the elemental proxies suggest phase II as a transition period, marked by progression towards a gradually wetter climate. This transition is extensively recorded in Rapa Nui archives as vegetation changes. Rano Aroi reflects a progressive expansion of palm woodland and shrubs to closed forests, along with the appearance of semi-aquatic vegetation, indicating a rise of the water table (Rull et al., 2015). Forest expansion would also improve pedogenetic processes and further reduce erosion, resulting in low lithogenic inputs as marked by PC1.

At a regional scale, the transition to a wetter climate in Rapa Nui is compatible with a southward shift of the ITCZ relative to its more northerly position during the MCA (Higley et al., 2018), corresponding with the low SST zonal gradient in the tropical Pacific (Conroy et al., 2010), and persistently negative SOI values marking El Niño-dominated conditions (Yan et al., 2011). These changes may characterize a period of intermediate transition from the MCA to the Little Ice Age (LIA), the latter placed by Nunn et al. (2007) from 1350 CE. However, the asynchronous timing among corresponding reconstructions (Fig. 8) makes it extremely difficult to infer specific causal dynamics and connections with the Rano Aroi record for this phase.

All of these climate-driven changes in the environmental fingerprint observed at the transition from phase I to phase II may coincide with the most-supported estimate for the arrival of first Polynesian colonizers between ~800 and ~1300 CE, although the possibility of multiple waves of arrivals prior to European contact (1722 CE) should not be excluded (Hunt and Lipo, 2006; Rull et al., 2018; Stevenson et al., 2015; Vargas et al., 2006; Wilmshurst et al., 2011). The correspondence between the early Polynesian arrival and the environmental transition may indicate travel to Rapa Nui was associated with favorable climatic conditions. Modified ocean circulation pathways, for example, may have facilitated travelling towards Rapa Nui through a 'climate corridor' with prevailing northwesterly winds (Goodwin et al., 2014; Sear et al., 2020), but this hypothesis remains unsupported by climatic models for eastern Pacific Ocean. Wetter conditions may also have favored the subsequent development of agricultural practices at Rapa Nui, especially in lowland areas of optimal rainfall and soil quality (Horrocks et al., 2015; Sear et al., 2020; Stevenson et al., 2015). Even if early agricultural development may have affected the local hydrological balance on the island, intensive agriculture near Rano Aroi did occur for several centuries later than phase II (Horrocks et al., 2015).

4.3. Phase III (1400–1520 CE)

Phase III is marked by indications of a shift to strongly wetter conditions. Lithogenic input increases (PC1) in conjunction with Ca (and Sr) (PC3), while K/Al markedly decreases suggesting that hydric erosion was accompanied by leaching and washout of the most mobile elements, and/or a significant uptake of K for primary production. The input of more weathered sediments is also supported by the clear peak in $(La/Yb)_N$ in this phase. A slight transition to a less anoxic environment is suggested by δCe and Mn/Fe, and partly by Fe/Al. The P/Al ratio reaches minimum values in this phase, suggesting less anoxic/more oxic conditions and/or a change in the plant community occupying the mire. This section of the core is also characterized by an increase in sedimentation rates. A rising water table may have promoted the expansion of plant macrophytes that, in turn, increased the formation of the peaty sediments.

The regional climate during phase III is characterized by a transition to conditions dominated by La Niña (Yan et al., 2011). The ITCZ moved to its southernmost position of the last two millennia during this period, possibly a consequence of changes in hemispheric temperature gradients driven by a decline in solar irradiance (Sachs et al, 2009, 2021). These changes accompanied the onset of the LIA, mostly marked as a pronounced cooling of northern hemisphere continents, which then persisted until ~1850. These processes are known to have profoundly influenced the rainfall regimes in the tropical Pacific but with complex spatio-temporal patterns and mechanisms which are still not completely understood. The limited availability of annually resolved and representative paleoclimatic archives from the region make fine-scale paleoclimatic reconstruction particularly challenging (Conroy et al., 2010; Sachs et al., 2009). Our record from Rano Aroi supports a clearly wetter of local climate during phase III which, again, is compatible with this overall scenario, but where local rather than synoptic factors are likely the primary drivers (Fig. 8).

In phase III, the number of inhabitants at Rapa Nui may have been as many as several thousand people (Brandt and Merico, 2015; Rull, 2016), although the model estimates of the number of inhabitants and the demographic dynamics are still poorly constrained. Nevertheless, evidence for human settlement and horticultural activity is still absent at Rano Aroi (Horrocks et al., 2015; Rull, 2016). Enhanced wet conditions and limited human pressure may have favored the expansion of palm forests during this period. This vegetation change is consistent with previous paleoenvironmental records for the site (Rull et al., 2015) but higher resolution pollen records are needed to support this interpretation.

4. 4Phase IV (1520–1710 CE)

Phase IV is characterized by a peak in Fe/Al values 10–20 times higher than the rest of the record that cannot be explained by only the contribution of exogenous coarser particles. Rather, the increase in Fe (and Mn, see PC2), is more likely a marker of strongly oxic conditions (Chesworth et al., 2006). The Mn/Fe ratio supports this conclusion. The low lithogenic input (PC1) of poorly weathered source material (K/Al and $(La/Yb)_N$), ascribable to physical weathering, in conjunction with a peak in Ca/Ti suggests a highly desiccated mire. These environmental changes may be directly related to a combination of a natural shift to arid conditions and to the expansion of horticultural activities at Rano Aroi starting in 1670 CE (Horrocks et al., 2015), that enhanced drainage of the mire and the associated desiccation. Evidence from the archaeological site of Ava Ranga Uka a Toroke Hau, in the middle section of the stream coming down from Rano Aroi to the southeast, also suggests massive hydraulic interventions in the area during this period, including a modified waterfall, paved platforms, channels, dams, a water basin made of dressed basalt, plantations of palm trees, all in a context interpreted as a long-term ritual related to water and trees (Vogt and Kühlem, 2017). The study of a soil profile near Rano Aroi associated early horticulture with covering the garden soil with a pavement of carved basalt stones and cobbles (Bork et al., 2019), even if the estimated age of ~1300 CE is inconsistent with our record.

Phase IV coincides with the middle of the LIA (Rull, 2016; Rull et al., 2018), which was characterized by widespread droughts, food, and social crises over parts of tropical Asia. This climatic period has been ascribed to a southern shift in the humid subtropical storm track with coincident stability of dry anticyclonic conditions over Rapa Nui (Mann et al., 2008; Sáez et al., 2009). On a regional scale, this period is characterized by a shift towards high intensity El Niño conditions that began earlier in the LIA (Yan et al., 2011). In other Pacific Ocean locations, this period has been marked by a southward shift in the position of the ICTZ, reaching close to the equator, which is 5° south of the modern position (Sachs et al., 2009). However, as mentioned above, large uncertainties remain in understanding the internal mechanisms of tropical Pacific hydroclimate on centennial-scales during this period, as are the effects at the local scale (Higley et al., 2018; Sachs et al., 2021). Sediments from Rano Raraku demonstrate that a prolonged desiccation of the lake occurred between 1570 and 1720 CE (Cañellas-Boltà et al., 2013), although the compression of last two millennia into less than 30 cm of sediment results in low-resolution data in this section of the core used by Cañellas-Boltà et al. (2013). These drought conditions may have affected the entire island including Ma'unga Terevaka, the highest elevation site on the island, located close to Rano Aroi, which is typically characterized by the highest precipitation on Rapa Nui (Puleston et al., 2017). Our record, particularly Fe/Al, Ca/Ti and P/Al signals (Fig. 8), consistently reflects this dry period between 1570 and 1720 CE. A similar dry signal was recorded by Rull et al. (2015, 2021) based on palynological and isotopic evidence (Fig. 8).

During phase IV Rano Aroi experienced its first but complete deforestation from 1520 CE to ~1650 CE, with palm forests and associated shrublands being replaced by grass meadows (Rull et al., 2015). This vegetation change was accompanied by an abrupt rise in charcoal accumulation, concomitantly observed in Rano Kau, that supports anthropogenic causes possibly exacerbated by climate change. Several authors argue that the climatic severity during the middle LIA may have shifted the baseline climatic conditions upon which the existing society relied, although this environmental and cultural link is likely complex (Rull et al., 2018 and references therein). As freshwater availability on the island is severely limited, droughts that lasted for ~150 years may have strongly contributed to trigger the Rapanui societal crisis.

4. 5Phase V (1710–1790 CE)

During phase V the elemental proxies mark a partial return of a hydroclimate system similar to the early LIA (phase III), with a relatively wetter climate and higher lithogenic input (PC1) but still predominantly oxic conditions (Fe/Al, Mn/Fe). These signals place the end of the LIA droughts in Rano Aroi in the first half of 18th century CE, in agreement with previous paleoclimatic studies on the island (Rull, 2021) and compatibly to the early re-positioning of the ITCZ towards northern latitude (1700–1870) (Sachs et al., 2009). According to our chronology, the time frame of phase V does not reach the end of the generally accepted window of late LIA at the scale of regional climate, 1850 CE (Thompson et al., 2013; Yan

et al., 2011), which thus could include encompass the subsequent phase VI.

The beginning of phase V approximatively coincides with the first European contact (1722 CE) (Dumont et al., 1998). Even if rapid cultural and environmental impacts due to this contact cannot be excluded, the biogeochemical changes recorded in Rano Aroi during this phase are likely related to climate and environmental variations. Although dry conditions were not as prominent as during phase IV, the limited availability of freshwater was still problematic for supporting human endeavors, as remarked upon in the subsequent expeditions of Spanish (1770 CE), British (1774 CE) and French (1786 CE) explorers (Dumont et al., 1998). Most of the forest conversion had already taken place by phase V and the cultural transition to the Birdman cult (Edwards and Edwards, 2013) along with the establishment of the cultural center at Orongo, near Rano Kau. The record from Rano Aroi shows a progressively wetter conditions, and/or interactions between increased precipitation and reduced horticultural activities associated with the general depopulation of Rapa Nui due to epidemic diseases (Hunt and Lipo, 2011).

4.6. Phase VI (1790–1900 CE)

Phase VI is characterized by a marked lithogenic input (PC1) of mineral sediments, as evidenced by the corresponding lighter colored unit (Fig. 2) and a decrease in the OC %. This decrease also corresponds to a depletion in Ca, Sr (PC3) and ΣREE (PC4), where the latter is indicative of more soluble elements (other than Ce, particularly in its oxidized form). Mn/Fe ratios indicate that mire conditions appear to be slightly less oxic than observed in the previous phase. The K/Al ratios indicate that the exogenous material is likely weathered, although $(La/Yb)_N$ does not show any significant change. The concomitant intense chemical weathering marked by K/Al and drop in the absolute levels of all REE (from PC4) despite a generally intense lithogenic input (PC1), combined with low mobility of Ce endogenously oxidized during phase IV is likely the cause of peaking δCe. Overall, the Rano Aroi record suggest that the climate during phase IV was considerably wetter than before, and characterized by intense hydric erosion favored by limited soil development and vegetation coverage due to previous droughts. Although direct anthropogenic factors cannot be excluded, intermittent occupation of humans at the Rano Aroi surroundings during this period makes human influence less likely to be responsible for these changes (Horrocks et al., 2015; Rull et al., 2015).

From the climatic perspective, phase VI with its intense precipitation events could be considered as the signal of late LIA termination, as much as phase III marked the onset of early LIA. Interestingly enough, our multielemental record from Rano Aroi seems to capture precisely both of such climatic transitions, where other records provide limited information individually (Thompson et al., 2013). The tendency of precipitation in Rano Aroi to be higher under stable conditions of the regional climate (neutral ENSO phases) may support this hypothesis, but further investigations are required.

4.7. Phase VII (1900 CE-Present)

Over the last century, the mire shifted to drier conditions. Human activities significantly impacted the Rano Aroi site, particularly through the creation of an earthen dike barrier and artificial outlet in the 1960s (Herrera and Custodio, 2008). These works altered transport dynamics and water level oscillations. Erosion of the outlet was also induced by introduction of sheep farming during much of the 20th century as well as the more recent grazing of roaming horses, resulting in consistent drying of the wetland system. The last century was marked by a strong decrease in Rapa Nui population as a result of environmental, societal and other interacting factors, such as the introduction of epidemic diseases and slave trading (McCall, 1993).

5. Conclusions

The decadal to multidecadal TE and REE records from Rano Aroi provides a coherent reconstruction of environmental changes that took place on Rapa Nui over the past two millennia. Cluster analysis and PCA identified seven distinct chronological phases marked by well-defined environmental transitions with connection to climatic factors. During the first millennium CE, when the island was uninhabited, K/Al, $(La/Yb)_N$ and the limited lithogenic input suggest that windy and relatively dry conditions may have generally prevailed. The redox state of the mire was anoxic, although not severe as previously assumed. From 1090 to 1400 CE, conditions became progressively wetter. This latter phase coincides with the arrival of the first Polynesians to Rapa Nui. Our record indicates significantly wetter conditions between 1400 and 1520 CE, marked by increased hydric erosion and compatibly with previous reconstructions on vegetation coverage (Rull et al., 2018). Our high-resolution record helps to refine the timing of the initiation and the extent of this wet phase at Rano Aroi, which corresponds to the early LIA. Between 1520 and 1710 CE, unprecedented higher values of Fe/Al, in conjunction with high K/Al and a peak in P/Al values, suggested that Rapa Nui was impacted by intense droughts, although low water levels in the Aroi mire may also be related to localized horticultural activities. We cannot exclude a possible link between cultural and non-cultural factors, as persistent droughts could have encouraged Rapanui to start horticulture practices and hydraulic works in the wetter higher elevation sites, including Rano Aroi. Droughts during this period have also been documented in Rano Raraku as a sedimentation hiatus. Contiguous sedimentation is recorded in our sediment core from the Aroi wetland during this period, suggesting that the higher elevations in the interior of the island were less impacted than the coastal lowlands. During the interval of first contact between Rapanui and Europeans, the climate shifted progressively to wetter conditions, culminating in a significant rainy phase between 1790 and 1900 CE, as indicated by an intense lithogenic inflows and chemical weathering associated to hydric erosion of previously oxidized soils and minerals. This second wet phase may mark the termination of late LIA at Rano Aroi. Sediment chemistry suggests that dry hydrological conditions prevailed at Rano Aroi during the last century, most probably driven by the creation of an earthen dike barrier and artificial outlet in 1960s, that altered transport dynamics and fluctuations in the water table.

Compared to previous studies, our higher-resolution record provides a more refined reconstruction of the environmental changes that took place at the Rano Aroi mire over the last 2000 years. Regional climate may have affected such changes by driving precipitation regimes through dynamics which are not systematic along the record: while intense droughts correspond to the middle LIA, dominated by La Niña, wet periods mark the early and late LIA, thus suggesting a potential sensitivity to neutral ENSO phases. These mechanisms require further investigation to be elucidated.

These reconstructions provide new information to disentangle the key questions raised on the relationship between environmental change and human activities:

(a) The major driver of biogeochemical and hydrological changes at Rano Aroi is the local rainfall regime, which exhibited high variability over the last two millennia. While wind and changing sea surface temperatures had some

influence, our data suggest precipitation was the primary driver of pedogenetic processes operating on the island. Precipitation influences the transport of exogenous elements into the mire, the level and stratification of the water table, internal recycling of nutrients and labile species, and the vegetation composition of the mire. At a centennial scale, distinctive phases in local rainfall regimes are qualitatively consistent with some reconstructions of regional climatic drivers, but substantial asynchronies among the few available records in the tropical Pacific make it impossible to coherently infer specific teleconnections.

(b-c) Although many of these changes are likely tied to intrinsic environmental variability, localized human influence cannot be excluded, especially related to changing horticultural activity at Rano Aroi. Rano Aroi remained undisturbed by human activities for centuries until 1520 CE, when vegetation burning practices led to a rapid and complete replacement of palms by grass meadows. Syntheses of archaeological data and oral traditions demonstrate that this transformation took place during a dramatic cultural shift for the Rapanui, accompanied by the expansion of settlements in the interior of the island. Elemental proxies from Rano Aroi exhibit an intense shift in the hydrological and geochemical equilibrium towards dry-oxic conditions between 1520 and 1710 CE, perhaps linked to the regional climate, which cannot be only ascribed to deforestation. It is nevertheless possible that the Rapanuis responded to a changing climatic pattern which was already in place, whose effects on the mire could have been exacerbated by their intervention.

Credit author statement

Marco Roman: Methodology, Formal analysis, Investigation, Writing – original draft David B. McWethy: Investigation, Writing – review & editing Natalie M. Kehrwald: Investigation, Writing – review & editing Evans Osayuki Erhenhi: Investigation Amy E. Myrbo: Investigation, Writing – review & editing, José M. Ramirez-Aliaga: Project administration, Writing – review & editing Anibal Pauchard: Writing – review & editing Clara Turetta: Investigation Carlo Barbante: Resources, Supervision Matthew Prebble: Writing – review & editing Elena Argiriadis: Investigation Dario Battistel: Conceptualization, Funding acquisition, Investigation, Formal analysis, Writing – original draft.

Declaration of competing interest

The authors declare that they have no known competing financial interests or personal relationships that could have appeared to influence the work reported in this paper.

Acknowledgements

This work was financially supported by the “The Last Tree Standing” grant from Ca’ Foscari University of Venice, Italy. The authors gratefully acknowledge Aygul Abdurrahimli for her support in the experimental activity and ELGA LabWater for providing the PURELAB Pulse and PURELAB Flex systems that produced the ultrapure water used throughout the study. Any use of trade, firm, or product names is for descriptive purposes only and does not imply endorsement by the U.S. Government.

Appendix A. Supplementary data

Supplementary data to this article can be found online at https://doi.org/10.1016/j.quascirev.2021.107115.

References

Allan, M., Le Roux, G., Piotrowska, N., Beghin, J., Javaux, E., Court-Picon, M., Mattielli, N., Verheyden, S., Fagel, N., 2013. Mid- and late Holocene dust deposition in western Europe: the Misten peat bog (Hautes Fagnes – Belgium). Clim. Past 9, 2285–2298. https://doi.org/10.5194/cp-9-2285-2013.

Anderson, A., Chappell, J., Gagan, M., Grove, R., 2006. Prehistoric maritime migration in the Pacific islands: an hypothesis of ENSO forcing. Holocene 16, 1–6. https://doi.org/10.1191/0959683606hl901ft.

Arnaud, F., Poulenard, J., Giguet-Covex, C., Wilhelm, B., Révillon, S., Jenny, J.P., Revel, M., Enters, D., Bajard, M., Fouinat, L., Doyen, E., Simonneau, A., Pignol, C., Chapron, E., Vannière, B., Sabatier, P., 2016. Erosion under climate and human pressures: an alpine lake sediment perspective. Quat. Sci. Rev. https://doi.org/10.1016/j.quascirev.2016.09.018.

Azizi, G., Flenley, J.R., 2008. The last glacial maximum climatic conditions on Easter Island. Quat. Int. 184, 166–176. https://doi.org/10.1016/j.quaint.2007.09.027.

Baker, P.E., Buckley, F., Holland, J.G., 1974. Petrology and geochemistry of easter island. Contrib. Mineral. Petrol. 44, 85–100. https://doi.org/10.1007/BF00385783.

Battistel, D., Roman, M., Marchetti, A., Kehrwald, N.M., Radaelli, M., Balliana, E., Toscano, G., Barbante, C., 2018. Anthropogenic impact in the Maya lowlands of petén, Guatemala, during the last 5500 years. J. Quat. Sci. 33, 166–176. https://doi.org/10.1002/jqs.3013.

Beer, J., Lee, K., Whiticar, M., Blodau, C., 2008. Geochemical controls on anaerobic organic matter decomposition in a northern peatland. Limnol. Oceanogr. 53, 1393–1407. https://doi.org/10.4319/lo.2008.53.4.1393.

Biester, H., Hermanns, Y.M., Martinez Cortizas, A., 2012. The influence of organic matter decay on the distribution of major and trace elements in ombrotrophic mires - a case study from the Harz Mountains. Geochem. Cosmochim. Acta 84, 126–136. https://doi.org/10.1016/j.gca.2012.01.003.

Blaauw, M., Christeny, J.A., 2011. Flexible paleoclimate age-depth models using an autoregressive gamma process. Bayesian Anal 6, 457–474. https://doi.org/10.1214/11-BA618.

Borgmark, A., Schoning, K., 2006. A comparative study of peat proxies from two eastern central Swedish bogs and their relation to meteorological data. J. Quat. Sci. 21, 109–114. https://doi.org/10.1002/jqs.959.

Bork, H.-R., Mieth, A., Newman, D., Haberkern, E., Hartl-Reiter, C., 2019. Easter island and the pacific: cultural and environmental dynamics. Proceedings of the 9th international conference on easter island and the pacific, held in the ethnological museum, Berlin, Germany: Burkhard Vogt (editor), annette Kühlem (editor), Andrea. In: Vogt, B., Kühlem, A., Mieth, A., Bork, H.-R. (Eds.), Easter Island and the Pacific: Cultural and Environmental Dynamics. Proceedings of the 9th International Conference on Easter Island and the Pacific. Rapanui Press.

Bowdery, D., 2015. An enigma revisited: identification of palm phytoliths extracted from the 1983 Rapa Nui, Rano Kao2 core. Veg. Hist. Archaeobotany 24, 455–466. https://doi.org/10.1007/s00334-014-0503-x.

Brandt, G., Merico, A., 2015. The slow demise of Easter Island: insights from a modeling investigation. Front. Ecol. Evol. 3, 13. https://doi.org/10.3389/fevo.2015.00013.

Bridgham, S.D., Updegraff, K., Pastor, J., 1998. CARBON, NITROGEN, and PHOSPHORUS MINERALIZATION IN NORTHERN WETLANDS, Ecology. John Wiley & Sons, Ltd. https://doi.org/10.1890/0012-9658(1998)079[1545:CNAPMI]2.0.CO;2.

Butler, K., Flenley, J., 2010. The Rano Kau 2 pollen diagram: palaeoecology revealed. Rapa Nui J 24, 5–10.

Butler, K., Prior, C.A., Flenley, J.R., 2004. Anomalous Radiocarbon Dates from Easter Island, in: Radiocarbon. University of Arizona, pp. 395–405. https://doi.org/10.1017/S0033822200039709.

Cañellas-Boltà, N., Rull, V., Sáez, A., Margalef, O., Bao, R., Pla-Rabes, S., Blaauw, M., Valero-Garcés, B., Giralt, S., 2013. Vegetation changes and human settlement of Easter Island during the last millennia: a multiproxy study of the Lake Raraku sediments. Quat. Sci. Rev. 72, 36–48. https://doi.org/10.1016/j.quascirev.2013.04.004.

Cañellas-Boltà, N., Rull, V., Sáez, A., Margalef, O., Giralt, S., Pueyo, J.J., Birks, H.H., Birks, H.J.B., Pla-Rabes, S., 2012. Macrofossils in Raraku Lake (Easter Island) integrated with sedimentary and geochemical records: towards a palaeoecological synthesis for the last 34,000 years. Quat. Sci. Rev. 34, 113–126. https://doi.org/10.1016/j.quascirev.2011.12.013.

Cañellas-Boltà, N., Rull, V., Sáez, A., Margalef, O., Pla-Rabes, S., Valero-Garcés, B., Giralt, S., 2016. Vegetation dynamics at Raraku lake catchment (easter island) during the past 34,000years. Palaeogeogr. Palaeoclimatol. Palaeoecol. 446, 55–69. https://doi.org/10.1016/j.palaeo.2016.01.019.

Chesworth, W., Cortizas, A.M., García-Rodeja, E., 2006. The redox–pH approach to the geochemistry of the Earth's land surface, with application to peatlands. In: Martini, I.P., Martínez Cortizas, A., Chesworth, W. (Eds.), Peatlands, Developments in Earth Surface Processes. Elsevier, pp. 175–195. https://doi.org/10.1016/S0928-2025(06)09008-0.

Conroy, J.L., Overpeck, J., Cole, J., 2010. El Niño/Southern Oscillation and Changes in the Zonal Gradient of Tropical Pacific Sea Surface Temperature over the Last 1.2

Ka, vol. 18. PAGES news, pp. 32–34. https://doi.org/10.22498/pages.18.1.32.
Damman, A.W.H., Tolonen, K., Sallantaus, T., 1992. Element retention and removal in ombrotrophic peat of Haeaedetkeidas, a boreal Finnish peat bog. Suo 25, 25008956.
Davranche, M., Gruau, G., Dia, A., Le Coz-Bouhnik, M., Marsac, R., Pédrot, M., Pourret, O., 2017. Rare earth elements in wetlands. In: Rinklebe, Jörg, Anna, Sophia, Knox, M.P. (Eds.), Trace Elements in Waterlogged Soils and Sediment. Taylor & Francis Group/CRC Press, pp. 135–162.
Diamond, J., 2005. Collapse: How Societies Choose to Fail or Succeed. Viking, New York.
Dumont, H.J., Cocquyt, C., Fontugne, M., Arnold, M., Reyss, J.L., Bloemendal, J., Oldfield, F., Steenbergen, C.L.M., Korthals, H.J., Zeeb, B.A., 1998. The end of moai quarrying and its effect on lake Rano Raraku, easter island. J. Paleolimnol. 20, 409–422. https://doi.org/10.1023/A:1008012720960.
Edwards, E., Edwards, A., 2013. When the Universe Was an Island - Exploring the Cultural and Spritual Cosmos of Ancient Rapa Nui. Hangaroa Press.
Elderfield, H., Greaves, M.J., 1982. The rare earth elements in seawater. Nature 296, 214–219. https://doi.org/10.1038/296214a0.
Ferrán, G., Mazzuoli, R., Lahsen Azar, A., González-Ferran, O., Mazzuoli, R., Lahsen, A., 2004. Geología del complejo volcánico isla de pascua, rapa nui, Chile, v región Valparaíso. Carta geológica-volcánica isla de pascua, in: U1989 c.1. Centro de Estudios Volcanológicos.
Ferrat, M., Weiss, D.J., Spiro, B., Large, D., 2012. The inorganic geochemistry of a peat deposit on the eastern Qinghai-Tibetan Plateau and insights into changing atmospheric circulation in central Asia during the Holocene. Geochem. Cosmochim. Acta 91, 7–31. https://doi.org/10.1016/j.gca.2012.05.028.
Flenley, J., Bahn, P., 2003. The Enigmas of Easter Island. Oxford University Press, Oxford.
Flenley, J.R., King, A.S.M., Jackson, J., Chew, C., Teller, J.T., Prentice, M.E., 1991. The late quaternary vegetational and climatic history of easter island. J. Quat. Sci. 6, 85–115. https://doi.org/10.1002/jqs.3390060202.
Flenley, J.R., King, S.M., 1984. Late quaternary pollen records from easter island. Nature 307, 47–50. https://doi.org/10.1038/307047a0.
Franzén, L.G., 2006. Mineral matter, major elements, and trace elements in raised bog peat: a case study from southern Sweden, Ireland and Tierra del Fuego, south Argentina. E.S.P. In: Martini, I.P., Martínez Cortizas, A., Chesworth, W.B.T.-D. (Eds.), Peatlands. Elsevier, pp. 241–269. https://doi.org/10.1016/S0928-2025(06)09011-0.
Geller, W., 1992. The temperature stratification and related characteristics of Chilean lakes in midsummer. Aquat. Sci. 54, 37–57. https://doi.org/10.1007/BF00877263.
Gioncada, A., Gonzalez-Ferran, O., Lezzerini, M., Mazzuoli, R., Bisson, M., Rapu, S.A., 2010. The volcanic rocks of Easter Island (Chile) and their use for the Moai sculptures. Eur. J. Mineral 22, 855–867. https://doi.org/10.1127/0935-1221/2010/0022-2057.
Glaser, P.H., Siegel, D.I., Reeve, A.S., Chanton, J.P., 2006. Hydrogeology of major peat basins in North America. E.S.P. In: Martini, I.P., Martínez Cortizas, A., Chesworth, W.B.T.-D. (Eds.), Peatlands. Elsevier, pp. 347–376. https://doi.org/10.1016/S0928-2025(06)09015-8.
Glynn, P.W., Wellington, G.M., Wieters, E.A., Navarrete, S.A., 2003. Reef-building Coral Communities of Easter Island (Rapa Nui), Chile, in: Latin American Coral Reefs. Elsevier B.V., pp. 473–494. https://doi.org/10.1016/B978-044451388-5/50021-7
Gonzalez-Ferran, O., 1987. Geological evolution of Chilean pacific oceanic islands. In: Castilla, J.C. (Ed.), Islas Oceanicas Chilenas: Conocimiento Cientifico y Necesidades de Investigacions. Ediciones Universidad Catolica de Chile, Santiago, pp. 37–53.
Goodwin, I.D., Browning, S.A., Anderson, A.J., Kirch, P.V., 2014. Climate windows for polynesian voyaging to New Zealand and easter Island. Proc. Natl. Acad. Sci. U. S. A 111, 14716–14721. https://doi.org/10.1073/pnas.1408918111.
Gossen, C., 2007. Report: the mystery lies in the Scirpus. Rapa Nui J 21.
Herrera, C., Custodio, E., 2008. Conceptual hydrogeological model of volcanic Easter Island (Chile) after chemical and isotopic surveys. Hydrogeol. J. 16, 1329–1348. https://doi.org/10.1007/s10040-008-0316-z.
Higley, M.C., Conroy, J.L., Schmitt, S., 2018. Last millennium meridional shifts in hydroclimate in the central tropical pacific. Paleoceanogr. Paleoclimatol. 33, 354–366. https://doi.org/10.1002/2017PA003233.
Horrocks, M., Baisden, W.T., Flenley, J., Feek, D., Nualart, L.G., Haoa-Cardinali, S., Gorman, T.E., 2012. Fossil plant remains at Rano Raraku, Easter Island's statue quarry: evidence for past elevated lake level and ancient Polynesian agriculture. J. Paleolimnol. 48, 767–783. https://doi.org/10.1007/s10933-012-9643-0.
Horrocks, M., Baisden, W.T., Harper, M.A., Marra, M., Flenley, J., Feek, D., Haoa-Cardinali, S., Keller, E.D., Nualart, L.G., Gorman, T.E., 2015. A plant microfossil record of Late Quaternary environments and human activity from Rano Aroi and surroundings, Easter Island. J. Paleolimnol. 54, 279–303. https://doi.org/10.1007/s10933-015-9852-4.
Horrocks, M., Marra, M., Baisden, W.T., Flenley, J., Feek, D., González Nualart, L., Haoa-Cardinali, S., Edmunds Gorman, T., 2013. Pollen, phytoliths, arthropods and high-resolution 14C sampling from Rano Kau, Easter Island: evidence for late Quaternary environments, ant (Formicidae) distributions and human activity. J. Paleolimnol. 50, 417–432. https://doi.org/10.1007/s10933-013-9735-5.
Hughes, P.D.M., Mauquoy, D., Barber, K.E., Langdon, P.G., 2000. Mire-development pathways and palaeoclimatic records from a full Holocene peat archive at Walton Moss, Cumbria, England. Holocene 10, 465–479. https://doi.org/10.1191/095968300675142023.
Hunt, T.L., 2007. Rethinking Easter Island's ecological catastrophe. J. Archaeol. Sci. 34, 485–502. https://doi.org/10.1016/j.jas.2006.10.003.
Hunt, T.L., Lipo, C., 2011. The Statues that Walked. Free Press, New York.
Hunt, T.L., Lipo, C.P., 2006. Late colonization of easter island. Science 80 (311), 1603–1606. https://doi.org/10.1126/science.1121879.
Ise, T., Dunn, A.L., Wofsy, S.C., Moorcroft, P.R., 2008. High sensitivity of peat decomposition to climate change through water-table feedback. Nat. Geosci. 1, 763–766. https://doi.org/10.1038/ngeo331.
Kellogg, L.E., Bridgham, S.D., 2003. Phosphorus retention and movement across an ombrotrophic-minerotrophic peatland gradient. Biogeochemistry 63, 299–315. https://doi.org/10.1023/A:1023387019765.
Koerselman, W., Verhoeven, J.T.A., 1992. Nutrient dynamics in mires of various trophic status: nutrient inputs and outputs and the internal nutrient cycle. In: Verhoeven, J.T.A. (Ed.), Fens and Bogs in the Netherlands. Springer Netherlands, pp. 397–432.
Krotz, L., Leone, F., Guido, G., 2016. High Accuracy of Nitrogen,Carbon and Sulfur Analysis for Agronomy Applications Using the Thermo Scientific Flash Smart Elemental Analyzer.
Le Roux, G., Laverret, E., Shotyk, W., 2006. Fate of calcite, apatite and feldspars in an ombrotrophic peat bog, Black Forest, Germany. J. Geol. Soc. London. 163, 641–646. https://doi.org/10.1144/0016-764920-035.
MacIntyre, F., 2001. ENSO, climate variability, and the Rapanui: Part 2. Oceanography and Rapa Nui. Rapa Nui J. J. Easter Isl. Found. 15.
Mann, D., Edwards, J., Chase, J., Beck, W., Reanier, R., Mass, M., Finney, B., Loret, J., 2008. Drought, vegetation change, and human history on Rapa Nui (isla de Pascua, easter island). Quat. Res. 69, 16–28. https://doi.org/10.1016/j.yqres.2007.10.009.
Margalef, O., Cañellas-Boltà, N., Pla-Rabes, S., Giralt, S., Pueyo, J.J., Joosten, H., Rull, V., Buchaca, T., Hernández, A., Valero-Garcés, B.L., Moreno, A., Sáez, A., 2013. A 70,000 year multiproxy record of climatic and environmental change from Rano Aroi peatland (Easter Island). Global Planet. Change 108, 72–84. https://doi.org/10.1016/j.gloplacha.2013.05.016.
Margalef, O., Martínez Cortizas, A., Kylander, M., Pla-Rabes, S., Cañellas-Boltà, N., Pueyo, J.J., Sáez, A., Valero-Garcés, B.L., Giralt, S., 2014. Environmental processes in Rano Aroi (Easter Island) peat geochemistry forced by climate variability during the last 70kyr. Palaeogeogr. Palaeoclimatol. Palaeoecol. 414, 438–450. https://doi.org/10.1016/j.palaeo.2014.09.025.
McCall, G., 1993. Little Ice age, some speculations for Rapanui. Rapa Nui J 7, 65–70.
Mieth, A., Bork, H.R., 2010. Humans, climate or introduced rats - which is to blame for the woodland destruction on prehistoric Rapa Nui (Easter Island)? J. Archaeol. Sci. 37, 417–426. https://doi.org/10.1016/j.jas.2009.10.006.
Mucciarone, D.A., Dunbar, R.B., 2003. Stable Isotope Record of El Niño-Southern Oscillation Events from Easter Island, in: Easter Island. Springer US, pp. 113–132. https://doi.org/10.1007/978-1-4615-0183-1_8.
Muller, J., 2006. Reconstructing Climate Change of the Last 55 Kyr: the Lynch's Crater Peat Mire Record. NE-QLD, Australia.
Muller, J., Kylander, M., Wüst, R.A.J., Weiss, D., Martinez-Cortizas, A., LeGrande, A.N., Jennerjahn, T., Behling, H., Anderson, W.T., Jacobson, G., 2008. Possible evidence for wet Heinrich phases in tropical NE Australia: the Lynch's Crater deposit. Quat. Sci. Rev. 27, 468–475. https://doi.org/10.1016/j.quascirev.2007.11.006.
Nelson, B.J., Wood, S.A., Osiensky, J.L., 2003. Partitioning of REE between Solution and Particulate Matter in Natural Waters: A Filtration Study, in: Journal of Solid State Chemistry. Academic Press Inc., pp. 51–56. https://doi.org/10.1016/S0022-4596(02)00145-7
Nunn, P.D., Hunter-Anderson, R., Carson, M.T., Thomas, F., Ulm, S., Rowland, M.J., 2007. Times of plenty, times of less: last-millennium societal disruption in the pacific basin. Hum. Ecol. 2007 354 (35), 385–401. https://doi.org/10.1007/S10745-006-9090-5.
Peteet, D., Beck, W., Ortiz, J., O'Connell, S., Kurdyla, D., Mann, D., 2003. Rapid Vegetational and Sediment Change from Rano Aroi Crater, Easter Island, in: Easter Island. Springer US, pp. 81–92. https://doi.org/10.1007/978-1-4615-0183-1_6.
Puleston, C.O., Ladefoged, T.N., Haoa, S., Chadwick, O.A., Vitousek, P.M., Stevenson, C.M., 2017. Rain, sun, soil, and sweat: a consideration of population limits on Rapa Nui (easter island) before European contact. Front. Ecol. Evol. 5, 69. https://doi.org/10.3389/fevo.2017.00069.
Rull, V., 2021. Contributions of paleoecology to Easter Island's prehistory: a thorough review. Quat. Sci. Rev. https://doi.org/10.1016/j.quascirev.2020.106751.
Rull, V., 2016. Natural and anthropogenic drivers of cultural change on Easter Island: review and new insights. Quat. Sci. Rev. https://doi.org/10.1016/j.quascirev.2016.08.015.
Rull, V., Cañellas-Boltà, N., Margalef, O., Sáez, A., Pla-Rabes, S., Giralt, S., 2015. Late Holocene vegetation dynamics and deforestation in Rano Aroi: implications for Easter Island's ecological and cultural history. Quat. Sci. Rev. 126, 219–226. https://doi.org/10.1016/j.quascirev.2015.09.008.
Rull, V., Cañellas-Boltà, N., Sáez, A., Giralt, S., Pla, S., Margalef, O., 2010. Paleoecology of easter island: evidence and uncertainties. Earth Sci. Rev. https://doi.org/10.1016/j.earscirev.2010.02.003.
Rull, V., Montoya, E., Seco, I., Cañellas-Boltà, N., Giralt, S., Margalef, O., Pla-Rabes, S., D'Andrea, W., Bradley, R., Sáez, A., 2018. CLAFS, a holistic climatic-ecological-anthropogenic hypothesis on easter island's deforestation and cultural change: proposals and testing prospects. Front. Ecol. Evol. 6, 32. https://doi.org/10.3389/fevo.2018.00032.
Sachs, J.P., Mügler, I., Sachse, D., Prebble, M., Wolhowe, M., 2021. Last millennium hydroclimate in the central equatorial North Pacific (5°N, 160°W). Quat. Sci. Rev.

Sachs, J.P., Sachse, D., Smittenberg, R.H., Zhang, Z., Battisti, D.S., Golubic, S., 2009. Southward movement of the Pacific intertropical convergence zone AD 1400-1850. Nat. Geosci. 2, 519–525. https://doi.org/10.1038/ngeo554.

Sáez, A., Valero-Garcés, B.L., Giralt, S., Moreno, A., Bao, R., Pueyo, J.J., Hernández, A., Casas, D., 2009. Glacial to holocene climate changes in the SE pacific. The Raraku lake sedimentary record (easter island, 27°S). Quat. Sci. Rev. 28, 2743–2759. https://doi.org/10.1016/j.quascirev.2009.06.018.

Schittek, K., Kock, S.T., Lücke, A., Hense, J., Ohlendorf, C., Kulemeyer, J.J., Lupo, L.C., Schäbitz, F., 2016. A high-altitude peatland record of environmental changes in the NW Argentine Andes (24 ° S) over the last 2100 years. Clim. Past 12, 1165–1180. https://doi.org/10.5194/cp-12-1165-2016.

Sear, D.A., Allen, M.S., Hassall, J.D., Maloney, A.E., Langdon, P.G., Morrison, A.E., Henderson, A.C.G., Mackay, H., Croudace, I.W., Clarke, C., Sachs, J.P., Macdonald, G., Chiverrell, R.C., Leng, M.J., Cisneros-Dozal, L.M., Fonville, T., 2020. Human settlement of East Polynesia earlier, incremental, and coincident with prolonged South Pacific drought. Proc. Natl. Acad. Sci. U. S. A 117, 8813–8819. https://doi.org/10.1073/pnas.1920975117.

Sherwood, S.C., Van Tilburg, J.A., Barrier, C.R., Horrocks, M., Dunn, R.K., Ramírez-Aliaga, J.M., 2019. New excavations in Easter Island's statue quarry: soil fertility, site formation and chronology. J. Archaeol. Sci. 111, 104994. https://doi.org/10.1016/j.jas.2019.104994.

Shotyk, W., 1996. Peat bog archives of atmospheric metal deposition: geochemical evaluation of peat profiles, natural variations in metal concentrations, and metal enrichment factors. Environ. Rev. https://doi.org/10.1139/a96-010.

Shotyk, W., 1988. Review of the inorganic geochemistry of peats and peatland waters. Earth Sci. Rev. 25, 95–176. https://doi.org/10.1016/0012-8252(88)90067-0.

Shotyk, W., Krachler, M., Martinez-Cortizas, A., Cheburkin, A.K., Emons, H., 2002. A peat bog record of natural, pre-anthropogenic enrichments of trace elements in atmospheric aerosols since 12 370 14C yr BP, and their variation with Holocene climate change. Earth Planet Sci. Lett. 199, 21–37. https://doi.org/10.1016/S0012-821X(02)00553-8.

Stevenson, C.M., Puleston, C.O., Vitousek, P.M., Chadwick, O.A., Haoa, S., Ladefoged, T.N., 2015. Variation in Rapa Nui (Easter Island) land use indicates production and population peaks prior to European contact. Proc. Natl. Acad. Sci. U. S. A 112, 1025–1030. https://doi.org/10.1073/pnas.1420712112.

Thompson, L.G., Mosley-Thompson, E., Davis, M.E., Zagorodnov, V.S., Howat, I.M., Mikhalenko, V.N., Lin, P.-N., 2013. Annually resolved Ice core records of tropical climate variability over the past ~1800 years. Science 80 (340), 945–950. https://doi.org/10.1126/SCIENCE.1234210.

Tipping, E., Benham, S., Boyle, J.F., Crow, P., Davies, J., Fischer, U., Guyatt, H., Helliwell, R., Jackson-Blake, L., Lawlor, A.J., Monteith, D.T., Rowe, E.C., Toberman, H., 2014. Atmospheric deposition of phosphorus to land and freshwater. Environ. Sci. Process. Impacts 16, 1608–1617. https://doi.org/10.1039/c3em00641g.

Tribovillard, N., Algeo, T.J., Lyons, T., Riboulleau, A., 2006. Trace metals as paleoredox and paleoproductivity proxies: an update. Chem. Geol. 232, 12–32. https://doi.org/10.1016/j.chemgeo.2006.02.012.

Vargas, P., Cristino, C., Izaurieta, R., 2006. 1.000 años en Rapa Nui: Arqueología del asentamiento humano en la Isla de Pascua. - Instituto de Asuntos Públicos - Universidad de Chile. Editorial Universitaria, Santiago.

Vogt, B., Kühlem, A., 2017. By the quebrada of Ava Ranga Uka A Toroke Hau – about landscape transformation and the significance of water and trees. In: Haoa Cardinali, S., Ingersoll, K.B., Ingersoll, D.W., Stevenson, C.M. (Eds.), Cultural and Environmental Change on Rapa Nui. Routledge, Oxford, New York, pp. 113–132.

Wilmshurst, J.M., Hunt, T.L., Lipo, C.P., Anderson, A.J., 2011. High-precision radiocarbon dating shows recent and rapid initial human colonization of East Polynesia. Proc. Natl. Acad. Sci. U. S. A 108, 1815–1820. https://doi.org/10.1073/pnas.1015876108.

Yan, H., Sun, L., Wang, Y., Huang, W., Qiu, S., Yang, C., 2011. A record of the Southern Oscillation Index for the past 2,000 years from precipitation proxies. Nat. Geosci. 4, 611–614. https://doi.org/10.1038/ngeo1231.

Zhang, M., Liu, Z., Xu, S., Sun, P., Hu, X., 2013. Element response to the ancient lake information and its evolution history of argillaceous source rocks in the Lucaogou Formation in Sangonghe area of southern margin of Junggar Basin. J. Earth Sci. 24, 987–996. https://doi.org/10.1007/s12583-013-0392-4.

Zhao, Y., Hölzer, A., Yu, Z., 2007. Late holocene natural and human-induced environmental change reconstructed from peat records in eastern central China. Radiocarbon 49, 789–798. https://doi.org/10.1017/S0033822200042661.

Zizka, G., 1991. Flowering Plants of Easter Island. Palmarum Hortus Francofortensis, Palmengarten.